Taylor & Francis
Taylor & Francis Group

Inhalation Toxicology
International Forum for Respiratory Research

ISSN: 0895-8378 (Print) 1091-7691 (Online) Journal homepage: https://www.tandfonline.com/loi/iiht20

Surface area- and mass-based comparison of fine and ultrafine nickel oxide lung toxicity and augmentation of allergic response in an ovalbumin asthma model

Katherine A. Roach, Stacey E. Anderson, Aleksandr B. Stefaniak, Hillary L. Shane, Vamsi Kodali, Michael Kashon & Jenny R. Roberts

To cite this article: Katherine A. Roach, Stacey E. Anderson, Aleksandr B. Stefaniak, Hillary L. Shane, Vamsi Kodali, Michael Kashon & Jenny R. Roberts (2019) Surface area- and mass-based comparison of fine and ultrafine nickel oxide lung toxicity and augmentation of allergic response in an ovalbumin asthma model, Inhalation Toxicology, 31:8, 299-324, DOI: 10.1080/08958378.2019.1680775

To link to this article: https://doi.org/10.1080/08958378.2019.1680775

Published online: 11 Nov 2019.

INHALATION TOXICOLOGY
2019, VOL. 31, NO. 8, 299–324
https://doi.org/10.1080/08958378.2019.1680775

Taylor & Francis
Taylor & Francis Group

RESEARCH ARTICLE

Surface area- and mass-based comparison of fine and ultrafine nickel oxide lung toxicity and augmentation of allergic response in an ovalbumin asthma model

Katherine A. Roach[a,b], Stacey E. Anderson[b], Aleksandr B. Stefaniak[c], Hillary L. Shane[b], Vamsi Kodali[d], Michael Kashon[e] and Jenny R. Roberts[b]

[a]School of Pharmacy, West Virginia University, Morgantown, WV, USA; [b]Allergy and Clinical Immunology Branch (ACIB), National Institute of Occupational Safety and Health (NIOSH), Morgantown, WV, USA; [c]Respiratory Health Division (RHD), NIOSH, Morgantown, WV, USA; [d]Pathology and Physiology Research Branch (PPRB), NIOSH, Morgantown, WV, USA; [e]BioAnalytics Branch (BB), NIOSH, Morgantown, WV, USA

ABSTRACT

Background: The correlation of physico-chemical properties with mechanisms of toxicity has been proposed as an approach to predict the toxic potential of the vast number of emerging nanomaterials. Although relationships have been established between properties and the acute pulmonary inflammation induced by nanomaterials, properties' effects on other responses, such as exacerbation of respiratory allergy, have been less frequently explored.

Methods: In this study, the role of nickel oxide (NiO) physico-chemical properties in the modulation of ovalbumin (OVA) allergy was examined in a murine model.

Results: 181 nm fine (NiO-F) and 42 nm ultrafine (NiO-UF) particles were characterized and incorporated into a time course study where measured markers of pulmonary injury and inflammation were associated with NiO particle surface area. In the OVA model, exposure to NiO, irrespective of any metric was associated with elevated circulating total IgE levels. Serum and lung cytokine levels were similar with respect to NiO surface area. The lower surface area was associated with an enhanced Th2 profile, whereas the higher surface area was associated with a Th1-dominant profile. Surface area-normalized groups also exhibited similar alterations in OVA-specific IgE levels and lung neutrophil number. However, lung eosinophil number and allergen challenge-induced alterations in lung function related more to particle size, wherein NiO-F was associated with an increased enhanced pause response and NiO-UF was associated with increased lung eosinophil burden.

Conclusions: Collectively, these findings suggest that although NiO surface area correlates best with acute pulmonary injury and inflammation following respiratory exposure, other physico-chemical properties may contribute to the modulation of immune responses in the lung.

Abbreviations: ALF: artificial lysosomal fluid; AUC: area under the curve; BAL: bronchoalveolar lavage; BALF: bronchoalveolar lavage fluid; BALT: bronchus-associated lymphoid tissue; BET: Brunauer-Emmett Teller; DAMP: damage-associated molecular pattern; DLS: dynamic light scattering; DM: dispersion media; FSEM: field scanning electron microscopy; GM-CSF: granulocyte macrophage colony stimulating factor; GS: Gamble's solution; ICP-MS: inductively-coupled plasma mass spectrometry; ICP-OES: inductively-coupled plasma optical emission spectrometry; IL: interleukin; LAL: limulus amebocyte lysate assay; LDH: lactate dehydrogenase; LN: lymph node; NiO: nickel oxide; NIOSH REL: National Institute of Occupational Safety and Health Recommended Exposure Limit; OSHA PEL: Occupational Safety and Health Administration Permissible Exposure Limit; OVA: ovalbumin; Penh: enhanced pause; PBS: phosphate buffered saline; TNF: tumor necrosis factor; XPS: X-ray photoelectron spectroscopy

ARTICLE HISTORY
Received 30 July 2019
Accepted 4 October 2019

KEYWORDS
Nanotoxicology; ovalbumin allergy model; nickel oxide nanoparticles; hypersensitivity; immune response

Introduction

Over the past several decades, advancements in nanotechnology have greatly expanded uses for engineered nanomaterials in diverse fields ranging from catalytics and electronics to pharmaceuticals and cosmetics. However, the physico-chemical properties unique to nanoscale materials that confer such utility have also been associated with unique interactions with biological systems that are not observed with their larger size counterparts. One of the major challenges presented by the rapid emergence of such large numbers of diverse nanomaterials is the vast amount of resources and time required to evaluate the safety of each material individually. Consequently, there has been a considerable amount of effort to delineate whether specific

CONTACT Katherine A. Roach WVQ1@cdc.gov Allergy and Clinical Immunology Branch (ACIB), National Institute of Occupational Safety and Health (NIOSH), 1095 Willowdale Drive, Morgantown, WV 26505, USA

nanomaterial physico-chemical properties correspond to mechanisms of toxicity and adverse outcome pathways. These relationships could then be used to preliminarily categorize the hazardous potential of emerging materials (Kuempel et al. 2012).

Efforts to correlate nanomaterial physico-chemical properties and toxicological modes of action have led to a better understanding of nanomaterial-induced pulmonary injury and inflammation following respiratory exposure. However, the physico-chemical properties associated with other adverse biological responses have not been explored to the same degree. The immune system has been shown to be a biological target of nanomaterials following all routes of exposure (Park et al. 2010; Lee et al. 2011; Cho et al. 2012a; De Jong et al. 2013). In this regard, metal-based nanomaterials are a particularly concerning entity since they are one of the classes of nanomaterials being manufactured in the largest quantities, and metals have been historically associated with diverse immunotoxicological effects (Vance et al. 2015). Although different immune responses to these materials have been investigated, there is a great deal of discrepancy in the studies that have focused on allergic response (Roach et al. 2019).

As the prevalence of allergic asthma continues to increase, asthmatic or atopic individuals represent a subpopulation that may be particularly susceptible to the adverse effects of metal nanomaterial exposure (Schneider et al. 2016). Likewise, the potential for respiratory exposure to metal nanomaterials to induce or exacerbate asthmatic conditions has become an area of active investigation. Several metal nanomaterials have been incorporated into asthma models and have been shown to augment numerous processes involved in the development and progression of allergic conditions (Meldrum et al. 2017). However, there are relatively few studies that examine the relationship between physico-chemical properties and these effects (Yoshida et al. 2011; Hirai et al. 2012; Ilves et al. 2014; Vandebriel et al. 2018). Subsequently, the capacity to identify emerging nanomaterials that present a particular risk with respect to asthma remains largely unaddressed.

The goal of these studies was to evaluate the pulmonary toxicity of nanoscale nickel, as well as determine if exposure has the capacity to augment allergic responses. Furthermore, the impact of various dose metrics on these responses was investigated. Accordingly, two sizes of NiO particles were administered to mice in doses normalized for mass and surface area. First, a time course study was performed to evaluate differences in pulmonary injury and inflammation induced by the materials at time points critical to the following study that examined allergic response. In the second study, the materials were incorporated into an OVA asthma model to determine if exposure to the particles prior to allergic sensitization and elicitation, as may occur in occupational settings, alters the allergic response. Subsequently, the relationship between NiO mass and surface area was able to be discerned with respect to pulmonary injury and inflammation, as well as augmentation of allergy.

Materials and methods

Material characterization

Two different sizes of nickel (II) oxide (NiO) particles were obtained from Sigma-Aldrich (St. Louis, MO). The primary particle sizes were reported by the manufacturer as 50 nm (ultrafine, NiO-UF) and −325 mesh (<44 µm, fine, NiO-F). Both materials were thoroughly characterized prior to incorporation into *in vivo* studies. Specific surface area and surface chemistry were assessed on the powder form of the particles. After suspension in delivery vehicle, size, morphology, agglomeration, zeta potential, surface reactivity, and presence of endotoxin were assessed.

Surface area

Surface area of the NiO particles was measured on the powder form by gas adsorption using a Micromeritics ASAP2020 surface area analyzer and ultra-high purity nitrogen adsorbate. Specific surface area was determined by using the multipoint Brunauer, Emmett, and Teller (BET) method (ASTM International 2002).

XPS analysis

Surface elemental composition was analyzed via X-ray Photoelectron Spectroscopy (XPS; Rocky Mountain Laboratories Inc., Golden, CO). XPS was performed both before and after sputter etching with a 2.0 keV Ar + ion beam, from which approximately 500 Å of material was removed from the surface. Analyses were performed with an Al ka X-ray source and charge neutralization of the sample surface was achieved with the use of a low-energy electron flood gun. Results were reported as relative surface elemental composition of C, O, Na, Cl, Si, Ni, and Br for each sample.

Particle preparation in dispersion medium

For *in vivo* studies, NiO particles were suspended in a physiologically compatible vehicle for delivery to mice. Concentrated stock solutions of NiO particles were prepared in USP-grade phosphate buffered saline (PBS) and sonicated for 10 s at 10 W with a probe sonicator. Stock suspensions were then diluted into dispersion media (DM, 0.6 mg/ml mouse serum albumin +0.01 mg/ml dipalmitoyl phosphatidyl choline in PBS), designed to mimic the biochemistry of the fluid lining the lung, prepared as described by Porter et al. (Porter et al. 2008). Dosing solutions were prepared at concentrations of 0.8 mg/ml for both the fine and ultrafine particles, and 0.06 mg/ml for the ultrafine particle, for delivery of a 40 µg and 3 µg dose, respectively. The 3 µg dose of the NiO-UF was calculated by normalizing the ultrafine surface area to that of the 40 µg dose of the fine particle. The samples were then sonicated at 10 W for 20 min on ice to dissipate heat generated from the sonication procedure.

Primary particle size, agglomerate size, and particle morphology

Field emission scanning electron microscopy (FESEM, Hitachi Model S-4800) was employed to assess primary particle size and morphology of the particles. NiO particles were prepared in DM for microscopic analysis. Images were collected for both particles and the diameters of 250 particles from each sample were recorded using point count methods. Image J Software (Version X; National Institutes of Health, Bethesda, MD) was used for analysis of mean diameter for each particle. For further analysis of average agglomerate size in delivery vehicle, samples were evaluated by dynamic light scattering (DLS, Microtrac, Inc., San Diego, CA) and hydrodynamic diameter was recorded.

Endotoxin contamination

Determination of endotoxin presence in NiO samples was assessed using the Pierce Limulus Amebocyte Lysate (LAL) Chromogenic Endotoxin Quantitation Kit (Thermo Scientific, Waltham, MA) according to the manufacturer's protocol. Both NiO samples were tested over multiple concentrations ranging from 5.0 to 0.25 μg/μl. Concentration of endotoxin was determined using a plate spectrophotometer at absorbance wavelength of 450 nm.

Zeta potential in DM

Zeta potential of NiO particles was determined by measuring electrophoretic mobility in DM (pH 7.4). All measurements were performed at 25 °C using a Malvern Zetasizer Nano ZS90 (Worcestershire, UK) equipped with a 633 nm laser at a 90° scattering angle. Samples were equilibrated inside the instrument for 2 min, and five measurements consisting of five runs each were recorded.

Dissolution potential

The rate of NiO dissolution was assessed for both particles in three simulated fluids representative of biological compartments that materials were most likely to associate with following their aspiration. NiO-F and NiO-UF were prepared by identical methods for *in vivo* dosing. An aliquot of each particle suspended in DM (pH 7.2) was retained for analysis, and the remaining suspension was divided and combined with either artificial lysosomal fluid (ALF, pH 4.5, representative of the biochemical environment following phagocytosis by alveolar macrophages) or Gamble's solution (GS, pH 7.4, representative of extracellular lung fluid), prepared according to previously-published procedures (Marques et al. 2011).

Triplicate samples of each particle suspended in DM, ALF, or GS were incubated at 37 °C and agitated daily. At 1, 10, 19, and 29 d, samples were centrifuged at 3500 rpm for 30 min, following which 2 mL of supernatant was removed and stored at 4 °C until analysis. The concentration of soluble Ni was assessed in each sample by inductively-coupled plasma optical emission spectrometry (ICP-OES). Samples were diluted to 5 mL and analyzed using a Perkin Elmer Optima 5300DV ICP to determine μg Ni/mL in each sample. Concentrations were averaged between triplicate samples and results were used to calculate the amount of soluble nickel released from the original dose with respect to time.

Animals

Specific pathogen-free female BALB/cJ mice, 6–8 weeks of age were obtained from Jackson Laboratory (Bar Harbor, ME) for use in the time course study and allergy model. The BALB/c strain is a Th2-responder commonly used to evaluate IgE-mediated allergy (Woolhiser et al. 2000; Klink and Meade 2003). All mice were housed individually in ventilated polycarbonate cages with HEPA-filtered air in the AAALAC-approved National Institute for Occupational Safety and Health (NIOSH) Animal Facility, and provided food (Harlan Teklad Rodent Diet 7913) and water ad libitum in a controlled humidity temperature environment with a 12 h light/dark cycle. Animals were allowed to acclimate for 1 week in the facility prior to exposures. All procedures in the studies comply with the ethical standards set forth by Animal Welfare Act and the Office of Laboratory Animal Welfare (OLAW). The studies were approved by the NIOSH Health Effects Laboratory Division (HELD) Institutional Animal Care and Use Committee within the Center for Disease Control and Prevention in accordance with an approved animal protocol (protocol number 16-JR-M-015).

In vivo exposure and study design

Dose determination

Occupationally relevant doses of NiO were calculated using the current OSHA-enforced permissible exposure limit (PEL, 1.0 mg/m^3 as an 8-h time weighted average) and NIOSH recommended exposure limit (REL, 0.015 mg/m^3 time weighted average) for insoluble nickel compounds. Assuming a 75 kg standard worker (31% sitting, 69% light exercise) and a 50 nm NiO particle (density: 6.67 g/cm^2) with a deposition efficacy of 31.2%, alveolar deposition was calculated as follows (ICRP 1994):

Equation 1 – Basic equation for standard worker lung deposition

$$\begin{aligned} &20\,000\ \text{mL/min (minute ventilation)} \\ &\times 10^{-6}\ \text{(air to liquid volume conversion)} \\ &\times 1.0\ \text{mg/m}^3\ \text{or}\ 0.015\ \text{mg/m}^3\ \text{(exposure limit)} \\ &\times 480\ \text{min (exposure time)} \\ &\times 0.312\ \text{(deposition efficiency)} \\ &= 2.995\ \text{mg/day at OSHA PEL, } 0.045\ \text{mg/day at NIOSH REL} \end{aligned}$$

The daily human alveolar deposition was then normalized to the surface area of the mouse lung and the number of exposure days at the PEL and REL were determined for a 40 μg dose using the following equation:

Equation 2 – Normalization of human lung deposition to surface area of mouse lung

2.995 mg/day at OSHA PEL, 0.045 mg/day at NIOSH REL $\times 0.065\ m^2$ (mouse lung surface area)/40 µg (selected dose) = 21 days at OSHA PEL, 1400 days at NIOSH REL

Accordingly, the 40 µg dose of NiO administered to mice was representative of 3 weeks of exposure at the current OSHA PEL and 4 years of exposure at the NIOSH REL. NiO-F and NiO-UF surface area measurements were then used to calculate doses normalized for both surface area and mass between particles, yielding three total NiO treatment groups: NiO-1 (40 µg NiO-F), NiO-2 (3 µg NiO-UF), and NiO-3 (40 µg NiO-UF).

Time course study

To evaluate the role of NiO particle size, mass, and surface area on pulmonary injury and inflammation at critical time points in the allergy model, a time course study was conducted. On day 0, three sets of mice were exposed by oropharyngeal aspiration to vehicle control (DM), 40 µg NiO-F, 3 µg NiO-UF, or 40 µg NiO-UF. Treatment groups and dose characteristics are shown in Table 1. Mice were fully anesthetized with isoflurane, placed on a slanted board, and suspended by the incisors. The mouth was opened, tongue moved aside, and a 50 µl aliquot of sample was pipetted on the base of the tongue. The animal was restrained until two full breaths were completed and returned to its cage, placed on its side, and monitored for recovery from anesthesia. Mice were humanely euthanized with an overdose of sodium pentobarbital euthanasia solution (100–300 mg/kg body weight; Fort Dodge Animal Health, Fort Dodge, IA) at 1, 10, 19, or 29 d post-exposure. The time points were selected as they corresponded to critical time points in the sensitization and challenge phases of the asthma model. The lungs from one set of mice ($n = 8$ per group per time point) underwent bronchoalveolar lavage (BAL) to collect fluid and cells for pulmonary toxicological analyses. In the same group of animals, serum was collected, and the spleen and mediastinal lymph nodes were harvested for cell counts and phenotyping. In another set of mice ($n = 6$ per group per time point), whole blood was taken for immune cell phenotyping and lungs were fixed with formalin for histopathological analysis. In the last set of mice ($n = 6$ per group per time point), lungs were isolated, lyophilized and used to evaluate lung burden of NiO (as described below) at the respective time points to determine particle clearance over time.

Table 1. NiO time course study treatment groups and corresponding exposure particle, size, dose mass, and dose surface area (SA).

Treatment Group	Particle	Primary particle size (nm)	Dose mass (µg)	Dose SA (mm^2)
DM	–	–	–	–
NiO-1	NiO-F	181	40	192
NiO-2	NiO-UF	42	3	192
NiO-3	NiO-UF	42	40	2580

Ovalbumin asthma model

In order to evaluate the potential for NiO to exacerbate allergy as a function of mass, surface area, and or size, the same NiO-F and NiO-UF doses from the time course study were incorporated into an OVA allergy model. On day 0, mice were exposed to vehicle control or NiO particles by oropharyngeal aspiration. On days 1 and 10, mice were sensitized to chicken egg OVA via intraperitoneal injection with alum adjuvant (0.9 µg OVA + 0.5 mg alum in 200 µl

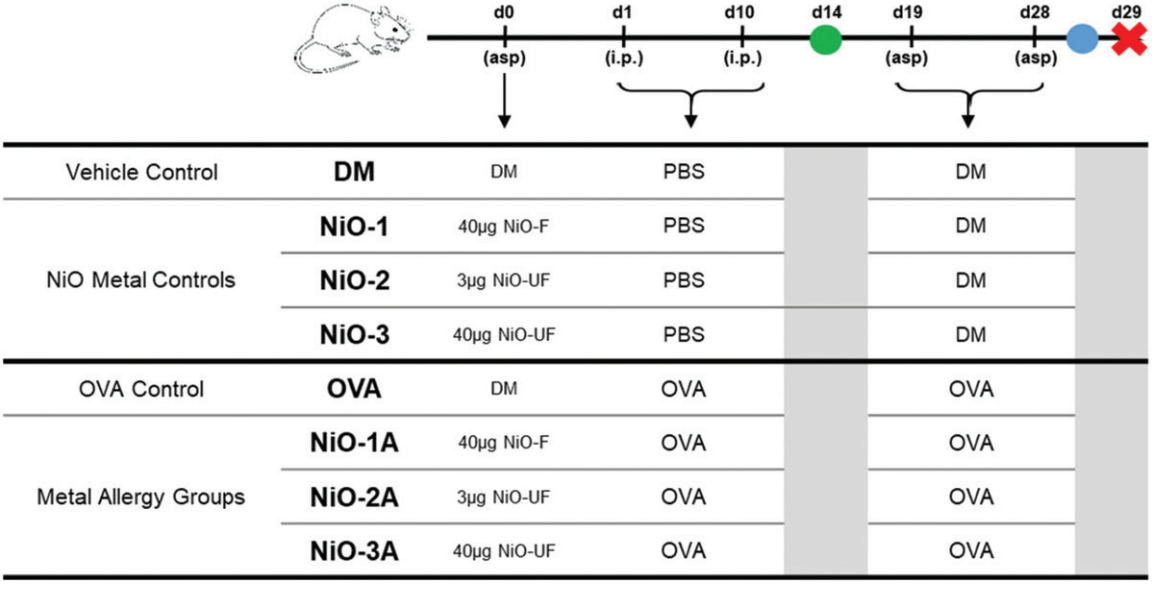

Figure 1. Treatment groups, corresponding exposures, and timeline of treatments in the OVA asthma model. Two groups of mice were exposed to dispersion medium (DM) or NiO particles at doses identical to those of the time course study on day 0 via oropharygenal aspiration (asp). One group of each treatment was not sensitized to OVA to serve as non-sensitized particle control groups and another group of each treatment was sensitized to OVA. Accordingly, on days 1 and 10, mice were intraperitoneally injected (i.p.) with PBS (non-sensitized) or OVA + alum in PBS (sensitized). On day 14, 150 µL blood was collected via the tail vein to evaluate circulating OVA-specific IgE levels, indicative of successful sensitization to OVA (green circle). On days 19 and 28, mice were aspirated with OVA or PBS and placed in whole body plethysmography (WBP) chambers to assess airway response to allergen challenge (blue circle). On day 29, all mice were euthanized.

PBS). Control animals were injected with 200 µl USP-grade PBS. A 150 µL aliquot of blood was collected from the tail vein of mice on day 14 to yield serum and confirm the presence of circulating OVA-specific IgE, indicative of successful sensitization. On days 19 and 28, mice were challenged via oropharyngeal aspiration to 50 µl sterile PBS or OVA (125 µg/50 µl sterile PBS) under isoflurane anesthetic. Directly following the second challenge (day 28) mice underwent whole body plethysmography to assess respiratory response to allergen challenge. Mice were euthanized on day 29 by sodium pentobarbital overdose. The study consisted of four particle exposure groups aspirated with DM, 40 µg NiO-F, 3 µg NiO-UF, or 40 µg NiO-UF on day 0, each with a non-sensitized particle control group and OVA-sensitized group, for a total of eight groups in the study. A schematic of the dosing regimen for this study is shown in Figure 1.

Post-allergen challenge lung function assessment

In the asthma model, airway response to allergen challenge was measured using an unrestrained whole body plethysmography system (Buxco Research Systems, Wilmington, NC). Directly following the second allergen challenge on day 28, mice were placed in individual plethysmograph chambers and given 5 min to acclimate prior to the start of measurements. Enhanced pause (P_{enh}), an indicator of airway resistance, was measured and recorded every 30 s for 6 h for each mouse. Following the completion of measurements, mice were returned to their cages and euthanized the following day. P_{enh} measurements from whole body plethysmography were plotted for each animal, area under the curve (AUC) was calculated, and mean AUC for each treatment group was calculated.

BAL cellular and fluid analysis

BAL was performed on the lungs in a set of mice from both the time course study and allergy model in order to obtain pulmonary cells for phenotypic analysis and fluid for analysis of biochemical indicators of lung injury and inflammation. Following euthanasia, the trachea was cannulated, the chest cavity was opened, and BAL was performed on the whole lungs. The acellular fraction of the first lavage was obtained by filling the lung with 0.6 ml PBS, massaging for 30 s, and withdrawing. This concentrated aliquot was retained, kept separate, and designated as the first fraction. The following aliquots were 0.6 ml in volume, instilled once with light massaging, withdrawn, and combined until a 2.4 ml volume was obtained. For each animal, both lavage fractions were centrifuged (10 min, 1600 rpm) and the cell pellets were combined and resuspended in 1 ml PBS for cell counts, phenotyping, and microscopic analysis. The acellular fluid from the first fraction was retained for analysis of LDH activity and quantification of cytokines.

The total numbers of BAL cells collected from mice were counted using a Coulter Multisizer II (Coulter Electronics, Hialeah, FL) within the size range of 4.5 µm and 20 µm. 75 000 cells were spun down onto slides for visual analysis with a Cytospin 3 centrifuge (Shandon Life Sciences International, Cheshire, England) and labeled with Leukostat stain (Fisher Scientific, Pittsburgh, PA) to differentiate alveolar macrophages, eosinophils, lymphocytes, and neutrophils. Another aliquot of cells were stained for surface markers for phenotype determination via flow cytometry as described below.

Measurements of LDH activity in BALF were obtained using a Cobas Mira analyzer (Roche Diagnostic Systems, Montclair, IN). LDH activity was quantified by detection of the oxidation of lactate coupled to the reduction of NAD + at 340 nm.

Lymphocyte differentials by flow cytometry

Lymph nodes (LN) and spleens were harvested from mice and processed between frosted microscope slides to yield single cell suspensions in sterile PBS. Concentrations of cells from each tissue were determined by identical methods used for enumeration of BAL cells.

Lymphocyte phenotypes were determined for BAL, LN, and spleen cells. 500 000 cells from each tissue were suspended in staining buffer (PBS + 1% bovine serum albumin + 0.1% sodium azide) containing F_c receptor blocking anti-mouse CD16/32 (BD Biosciences). Cells were incubated for 5 min, washed, and resuspended in staining buffer containing fluorochrome-conjugated antibodies. BAL, LN and spleen cells were stained with a panel of cell surface markers for lymphocyte-differentiation. CD2-BV605, CD3-APC, CD4-FITC, CD8-PE, CD44-APC-R700, CD45-PerCP, CD45R(B220)-PE-Cy7, and CD86-BV421 (BD Biosciences) were used to discriminate between populations of CD4+ T-lymphocytes, CD8+ T-lymphocytes, B-lymphocytes, and NK cells, as well as determine the corresponding activation state. An additional aliquot of BAL cells was stained with a second panel of markers to allow for differentiation of myeloid cell subsets. CD11b-PE-CF594, CD11c-APC-R700, CD24-BV605, CD45-PerCP, CD64-PE, CD86-PE-Cy7, MHC II-BV515, Ly6G-APC, Siglec-F-APC-Cy7 (BD Biosciences) were employed to differentiate between eosinophils, neutrophils, macrophages, and dendritic cells (Misharin et al. 2013). Cells were incubated for 30 min, washed, and fixed in 100 µl Cytofix Buffer (BD Biosciences). Compensation controls were prepared using corresponding cell types stained with a single fluorophore. For each sample, 100 000 events were recorded on an LSR II flow cytometer (BD Biosciences, San Diego, CA). In all analysis, doublet exclusion was performed and cellular populations were gated on using FSC-A x SSC-A parameters, prior to subsequent analysis. All data analysis was performed using FlowJo 7.6.5. Software (TreeStar Inc., Ashland, OR).

BAL fluid and serum proteins

Cytokines in the BAL fluid and serum of mice in the time course study and allergy model were quantified using a Milliplex MAP Kit magnetic bead panel (EMD Millipore

Corporation, Billerica, MA) and analyzed on a Luminex 200 system (Luminex Corporation, Austin, TX). For both studies, cytokines analyzed included interleukin (IL)-2, 4, 5, 6, 10, 12p40, 12p70, 13, 17, eotaxin, tumor necrosis alpha (TNF-α), interferon gamma (IFN-γ), and granulocyte macrophage colony stimulating factor (GM-CSF).

Levels of circulating total and OVA-specific IgE were assessed by ELISA in serum collected at 14 and 29 d in the allergy model. Serum was diluted 1:10 and total IgE was assessed using the Mouse IgE ELISA kit (Innovative Research, Novi, MI) according to manufacturer instructions. Serum was diluted 1:25 and assessed for OVA-specific IgE levels using the Anti-Ovalbumin IgE (mouse) ELISA Kit (Caymen Chemical Company, Ann Arbor, MI) according to the manufacturer's specifications.

Lung histopathology and particle clearance

For histopathological analysis, whole lungs from mice in the time course study and allergy model ($n = 6$ per group per time point) were inflated with 10% neutral buffered formalin for fixation, paraffin embedded, sectioned, and stained with hemotoxylin and eosin stain. Slides were quantitatively analyzed by a certified veterinary pathologist (Charles River Laboratories, Frederick, MD), who was blinded to the treatment groups. Indices of inflammation, injury, and fibrosis were scored on scale of 0–5, where 0 = no observed effect, 1 = minimal response, 2 = mild response, 3 = moderate response, 4 = marked response, and 5 = severe response, for both studies. For histopathology in the OVA models, additional parameters with relevance to allergic disease were assessed, including thickening around airways (epithelium and or smooth muscle), eosinophil and lymphocyte influx, and development of bronchus-associated lymphoid tissue (BALT).

To determine the rate of NiO-F and NiO-UF clearance from the lung, whole lungs ($n = 6$ per group) from mice in the time course study were isolated, lyophilized, and weighed to obtain the dry weight. Concentration of nickel in lung tissue 1, 10, 19, and 29 d post-exposure was determined by inductively-coupled plasma mass spectrometry (ICP-MS; ALS Environmental, Kelso, WA) and reported as μg Ni/mg tissue. This information was then multiplied by the dry weight of the whole lungs for each animal, expressed as percent Ni mass of originally-administered dose (40 μg) remaining at each time point, and averaged for each group.

Statistical analysis

Statistical analyses were conducted with GraphPad Prism version 7 (San Diego, CA). Results from all studies are expressed as means ± standard error and considered statistically significant at $p < 0.05$. For the time course study, treatments were compared by one-way analysis of variance (ANOVA) followed by a *post hoc* Student's *t*-test. All treatment groups from the allergy model, irrespective of sensitization status, were compared using ANOVA and Student's *t*-test. For some endpoints in the OVA model, NiO-exposed/OVA-sensitized groups were analyzed independently of non-sensitized groups, and results were presented as fold-change over OVA control levels. Histology scores were analyzed using nonparametric Wilcoxon rank-sum tests using JMP version 13 (SAS Institute, Cary NC) ($p < 0.05$).

Table 2. Summary of NiO-F and NiO-UF characterization data.

	NiO-F	NiO-UF
Vendor size specification	−325 mesh	50 nm
Primary particle size (FESEM)	181 ± 37 nm	42 ± 7 nm
Average agglomerate size		
FESEM	640 nm	190 nm
DLS	321 nm	109 nm
Morphology	irregular, jagged	spherical
Specific surface area (m^2/g)	4.79 ± 0.27	64.49 ± 2.98
Ni: O ratio	1:1	1:1.3
Endotoxin level	ND	ND
Zeta Potential (mV)	−8.42 ± 2.20	−6.23 ± 2.45

ND: Not Detected.

Results

Material characterization

Using FESEM microscopic images, 250 particles were measured to determine average primary particle size of both NiO particles. Measurements indicated an average primary particle size of 181 nm and 42 nm for NiO-F and NiO-UF, respectively. Average agglomerate size in DM was also measured in the micrographs and was found to be 640 nm for NiO-F and 190 nm for NiO-UF. DLS measurements also indicated a size difference in agglomerates, reporting hydrodynamic diameters of 321 nm for NiO-F and 109 nm for NiO-UF. Size characteristics are reported in Table 2. Microscopic analysis of NiO-F and NiO-UF particles also revealed differing morphologies between the two materials. NiO-F particles were generally jagged with a layered appearance (Figure 2(A)), whereas NiO-UF particles were consistently spherical in shape (Figure 2(B)) with a comparatively smoother surface structure.

Specific surface areas of the particles measured by BET analysis were 4.79 ± 0.27 m^2/g for NiO-F and 64.49 ± 2.98 m^2/g for NiO-UF particles. XPS analysis showed similar surface chemistries between NiO-F and NiO-UF particles with compositions consisting primarily of nickel and oxygen with various trace elements detected. Slight variations in nickel:oxygen ratios between NiO-F and NiO-UF samples were observed (1:1 and 1:1.3, respectively). Assessment of endotoxin presence on NiO particles confirmed undetectable levels (below 0.1 EU/ml) in both samples.

NiO-F and NiO-UF dissolution kinetics were shown to be dependent on the pH of the suspension fluid (Figure 3). Minimal release of ions was observed from either particle when suspended in DM or GS, irrespective of time. However, suspension of particles in ALF was associated with increased dissolution and time-dependent increases in

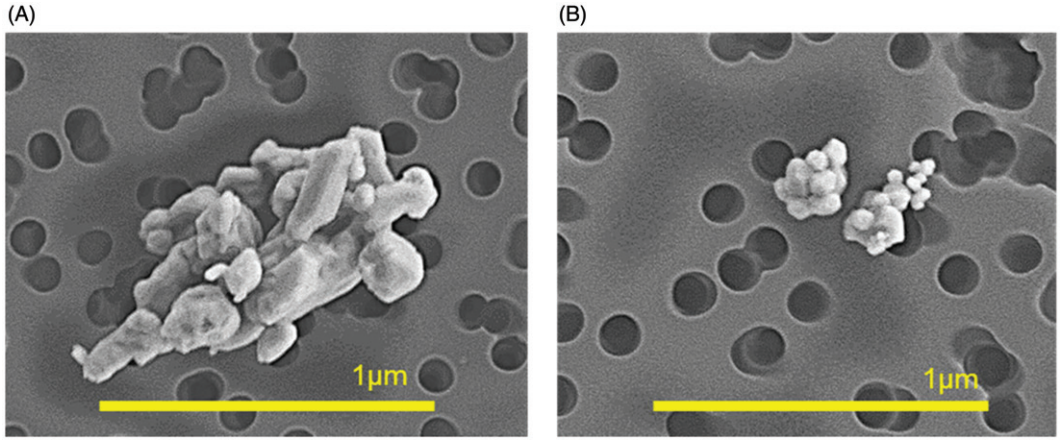

Figure 2. Electron micrographs of NiO-F (A) and NiO-UF (B) particles in DM illustrating size and morphology differences.

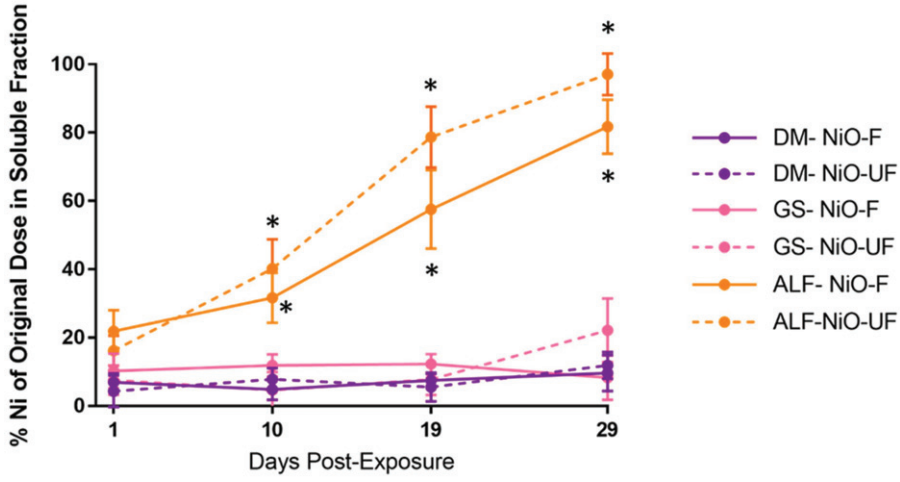

Figure 3. Rate of dissolution for NiO-F (solid lines) and NiO-UF (dotted lines) in different simulated biological fluids shown as percent of the original Ni concentration measured as soluble fraction. Purple lines represent particles suspended in dispersion media (DM, pH 7.2), pink lines indicate particles suspended in Gamble's solution (GS, pH 7.4), and orange lines indicate particles suspended in artificial lysosomal fluid (ALF, pH 4.5). $n = 3$, $p < 0.05$, * indicates statistically different from the same particle in GS and DM suspensions.

the concentration of nickel ions released. No statistically significant differences in the rate of dissolution were observed between NiO-F and NiO-UF at any time point, irrespective of physiological media type.

Collective findings from physico-chemical characterization of NiO-F and NiO-UF are summarized in Table 2.

NiO time course study

Mice were oropharyngeally aspirated with a single dose of NiO-F or NiO-UF in doses normalized for particle mass (40 µg) or surface area (1.92 mm, 3 µg) and euthanized 1, 10, 19, or 29 d post-exposure for evaluation of pulmonary toxicity. Exposure groups for the time course study and corresponding metrics of each NiO dose are shown in Table 1.

Evaluation of pulmonary injury and inflammation

The degree of particle-induced pulmonary injury and inflammation was assessed by quantification of lavage fluid LDH levels, total BAL cell number, and number of BAL neutrophils at all time points (Figure 4). No statistically significant alterations in any of these parameters were observed 1 d post-aspiration. Among the time points examined in this study, NiO-induced injury and inflammation was greatest for all groups at 10 d post-aspiration. When administered in mass-equivalent doses of 40 µg, NiO-UF (NiO-3 group) induced a greater degree of lung injury and inflammation than NiO-F (NiO-1 group). LDH was significantly elevated in the NiO-3 group compared to all other groups at 10 and 19 d (Figure 4(A)). LDH was elevated in the NiO-1 group at 10 d, only when compared to control, and it did not differ from the NiO-2 group, for which dose was normalized to the surface area of NiO-1. LDH levels returned to control values by 29 d for all groups. No significant increases in total BAL cell number (Figure 4(B)) or lung neutrophils (Figure 4(C)) were observed in the NiO-1 or NiO-2 groups, which had similar surface area by dose, when compared to control (or each other) at any time point in the study. However, the NiO-3 group exhibited significantly increased numbers of total BAL cells and lung neutrophils

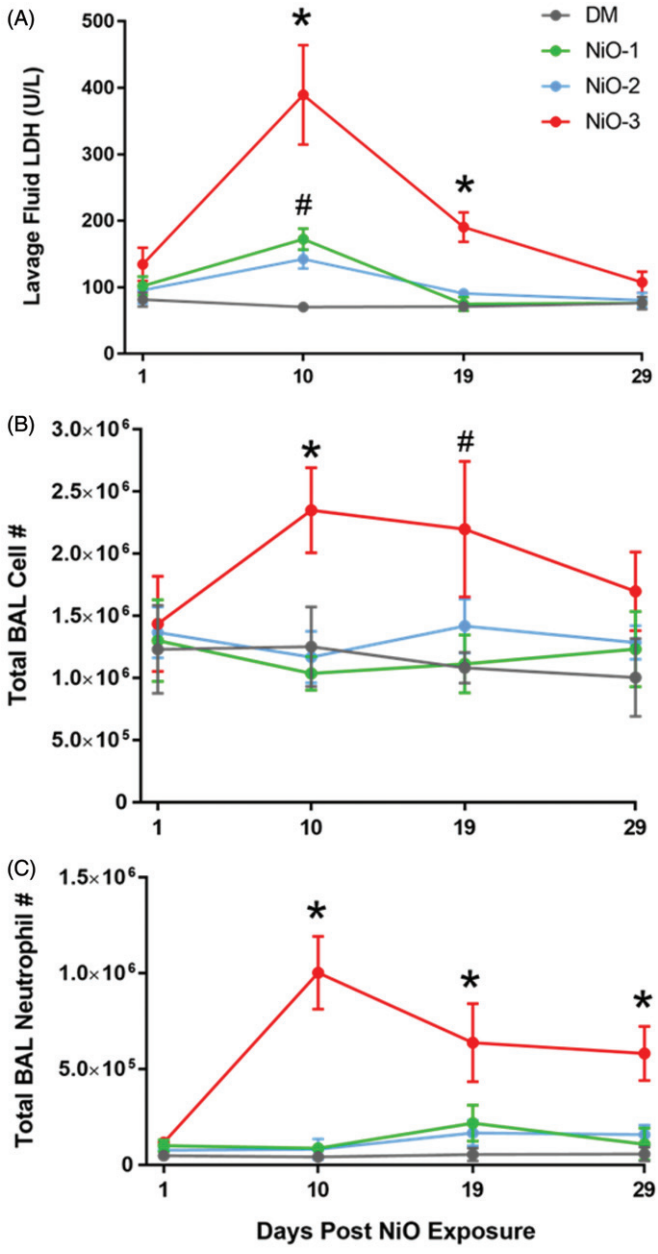

Figure 4. Markers of pulmonary injury and inflammation measured in mice from the NiO time course study at 1, 10, 19, and 29 d post NiO exposure following bronchoalveolar lavage (BAL). (A) Lung lactate dehydrogenase (LDH) levels in BAL fluid; (B) total cell number in BAL; and (C) total neutrophil number in BAL are shown for DM control (gray), NiO-1 (green), NiO-2 (blue), and NiO-3 (red) groups. $n = 8$, $p < 0.05$, * indicates statistically significant from all other groups, # indicates statistically significant from DM control.

at 10 d, and lung neutrophil number remained significantly elevated compared to all groups for the duration of the time course.

Total lymph node cell number and cell phenotyping

Similar to the measures of lung injury and inflammation, variations in mediastinal lymph node size and cellular composition were observed in response to the mass-normalized doses of NiO-F and NiO-UF. When administered at 40 µg, NiO-UF exposure (NiO-3 group), which had the highest surface area by dose, caused an earlier onset and persistence of lymph node expansion, as well as a significantly greater maximal cell number at 10 and 19 d, when compared to the same mass-based dose of NiO-F (NiO-1 group) (Figure 5(A)). Lymphocyte numbers in the surface area-normalized doses, NiO-1 and NiO2, significantly increased over control beginning at 19 d, but did not differ significantly from each other at 1, 10, or 19 d. However, at 29 d lymph node expansion continued in the NiO-2 group to a similar level as the NiO-3 group, and this did not occur in the NiO-1 group. Despite the increases observed in total lymphocyte cell numbers, ratios of lymphocyte phenotypes did not differ significantly between groups at any time point (Figure 5(B)). A similar trend was observed with respect to lymphocyte populations in the spleen (data not shown).

Cytokine analysis

BALF cytokine levels in each group at each time point were consistent with the corresponding inflammatory response illustrated by other measures of toxicity. Generally, cytokine responses were surface area-dependent. Exposure to the higher surface area-based dose resulted in more pronounced and persistent increases in several pro-inflammatory cytokines in the BALF (Table 3), including IL-6, IFN-γ, and TNF-α which persisted until the final endpoint (Figure 6).

Serum cytokine levels demonstrated a similar trend as BAL fluid cytokines (Table 3). However, significant differences over DM control levels were only observed in the NiO-3 group with respect to TNF-α at 19 d and IFN-γ at 1, 10, and 19 d.

Lung histopathology and particle clearance

Histopathological analysis of lung tissue from DM controls and animals exposed to the 40 µg dose of fine particle (NiO-1) and the ultrafine particle (NiO-3) were evaluated for markers of injury and inflammation by a board-certified veterinarian who was blinded to treatment groups (Table 4). Findings confirmed the presence of particles in alveolar macrophages of all NiO-exposed groups, the temporal progression of which corresponded to microscopic and ICP-MS analysis and Ni clearance findings discussed below. The degree of inflammatory cell infiltration reported by the histopathological analysis was also in accordance with the findings from differential phenotyping performed by flow cytometry. Peribronchiolar/perivascular edema and cellular accumulation was more severe in animals exposed to NiO-3 compared to NiO-1, and NiO-3-induced tissue injury was still prominent 29 d post-exposure.

To evaluate particle clearance over time, a separate group of animals were exposed to a mass-normalized 40 µg dose of either particle (representative of the NiO-1 and NiO-3 groups). Subsequently, Ni lung burden was measured at 1, 10, 19, and 29 d post-exposure (Figure 7). Results showed that lung Ni levels were comparable between animals exposed to both particles 1 d post-exposure; however, by 10 d, lungs of animals exposed to the fine particle contained 62% of the original dose, whereas lungs of animals exposed to the ultrafine particle only contained 47% of the original

(A)

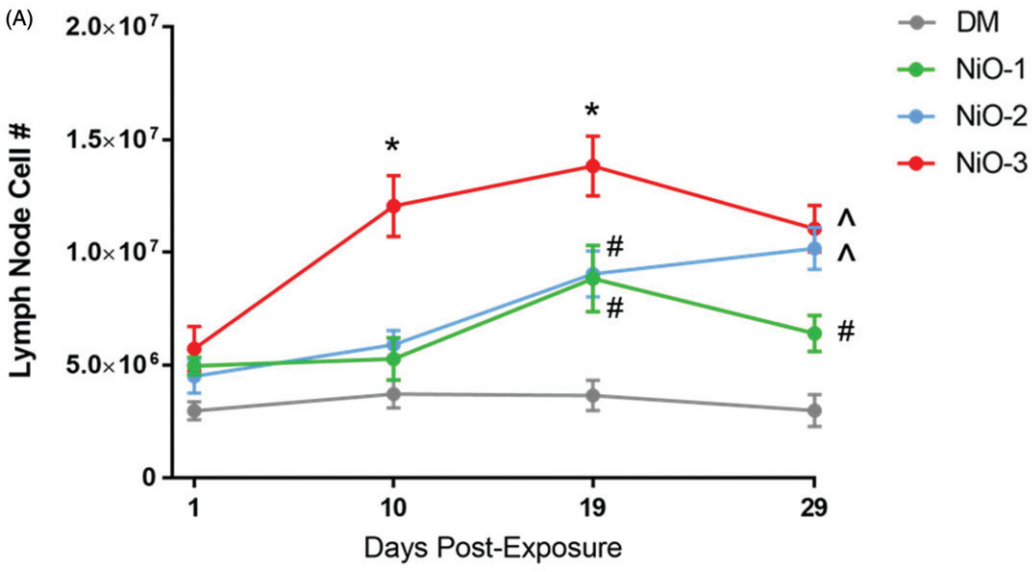

(B)

NiO Time Course Study
Lymph Node Cell Phenotypes by Percent of Total Cells

Time	Group	Total Cell # (x10^6)	Cell Populations by Phenotype (% of total cells)			
			CD4+ T-cells	CD8+ T-cells	B-cells	Other
1d	DM	3.33 ± 1.51	51.6 ± 4.56	21.1 ± 2.33	15.1 ± 2.22	12.2 ± 3.2
	NiO-1	4.70 ± 1.61	52.3 ± 6.21	19.8 ± 2.98	14.2 ± 2.10	13.7 ± 2.1
	NiO-2	4.81 ± 1.44	53.4 ± 4.14	20.0 ± 3.02	16.5 ± 3.12	10.1 ± 1.8
	NiO-3	5.70 ± 2.20	49.7 ± 7.85	21.2 ± 2.24	12.3 ± 1.74	16.8 ± 2.1
10d	DM	3.09 ± 1.51	51.8 ± 5.55	20.6 ± 2.56	14.4 ± 2.01	13.2 ± 2.2
	NiO-1	5.08 ± 1.62	48.6 ± 5.47	23.4 ± 3.02	15.5 ± 1.66	12.5 ± 2.1
	NiO-2	5.22 ± 1.64	49.9 ± 5.12	20.8 ± 3.11	17.7 ± 1.04	11.6 ± 2.0
	NiO-3	11.96 ± 3.11 *	47.5 ± 6.23	20.9 ± 2.13	16.4 ± 3.17	15.2 ± 2.2
19d	DM	3.64 ± 1.34	53.0 ± 7.45	24.5 ± 3.64	15.0 ± 2.25	7.5 ± 1.5
	NiO-1	8.27 ± 2.17 #	50.7 ± 5.12	22.1 ± 3.02	15.2 ± 2.77	12.0 ± 2.6 #
	NiO-2	8.41 ± 3.29 #	50.1 ± 6.11	22.7 ± 2.99	14.2 ± 2.09	13.0 ± 2.7 #
	NiO-3	13.28 ± 2.34 *	51.1 ± 5.23	20.8 ± 2.47	16.2 ± 2.11	11.9 ± 1.9 #
29d	DM	2.98 ± 1.02	54.0 ± 4.11	20.9 ± 2.66	15.5 ± 1.98	9.6 ± 1.8
	NiO-1	6.26 ± 1.97 #	50.0 ± 6.10	21.9 ± 3.07	14.2 ± 2.08	13.9 ± 1.1 #
	NiO-2	9.51 ± 2.11 ^	52.2 ± 5.05	21.1 ± 4.03	13.9 ± 1.46	12.8 ± 2.9 #
	NiO-3	10.71 ± 3.31 ^	53.1 ± 4.99	20.3 ± 2.70	12.8 ± 1.77	13.8 ± 3.0 #

Figure 5. (A) Total cell number in the mediastinal lymph node recovered from each group and (B) cell phenotypes by percent at 1, 10, 19, and 29 d post-exposure in the NiO time course study. $n = 8$, $p < 0.05$, * indicates statistically significant from all other groups, # indicates statistically significant from DM, ^ indicates statistically significant from DM and NiO-1.

dose Ni mass. At 19 d and 29 d post-exposure, lungs from both groups contained approximately 39% and 32% of the original Ni dose mass, respectively.

Dark field microscopy and light microscopy were used to visualize the particle burden in alveolar macrophages with respect to time post-exposure. Collectively, the degree of particle loading and frequency of particle-laden alveolar macrophages in each group appeared consistent with the clearance data obtained from the whole lung Ni burden analysis. Figure 8 shows images of particle-laden alveolar macrophages from each group 10 d post-exposure.

OVA asthma model

For the OVA asthma model, animals were administered the same NiO doses from the time course study by oropharyngeal aspiration on 0 d. On 1 and 10 d, mice were sensitized to OVA (OVA, NiO-1A, NiO-2A, and NiO-3A groups), or administered vehicle to serve as non-sensitized control groups (DM, NiO-1, NiO-2, and NiO-3 groups). Aspiration OVA challenge occurred on 19 and 28 d, lung function was measured following the second challenge, and mice were euthanized the following day. Treatment groups, corresponding exposures, and timeline of treatments for the OVA study are shown in Figure 1.

Day 14 post-sensitization serum IgE evaluation

Following NiO aspiration and two sensitization procedures, levels of circulating total IgE and OVA-specific IgE were evaluated on 14 d to confirm successful sensitization of allergy groups (Figure 9). Total IgE levels were elevated in all sensitized groups compared to non-sensitized groups at 14 d. The presence of OVA-specific IgE exclusively in all sensitized groups indicated successful sensitization to OVA. No statistically significant differences in total or OVA-specific IgE levels were observed between any groups with shared sensitization status.

Table 3. Raw values of serum and BALF cytokine levels for each treatment group at 1, 10, 19, and 29 d post NiO aspiration in the NiO time course study.

		IFN-γ	IL-2	IL-12p40	IL-12p70	IL-17	TNF-α	GM-CSF	IL-4	IL-5	IL-13	Eotaxin	IL-6	IL-10
Serum														
1d	DM	10.1 ± 2.1	4.4 ± 1.4	43.2 ± 16.2	25.7 ± 13.6	12.0 ± 1.7	8.0 ± 2.4	34.2 ± 5.0	7.6 ± 2.1	31.4 ± 5.1	50.1 ± 16.2	420 ± 45.2	42.3 ± 15.4	16.0 ± 2.1
	NiO-1	11.2 ± 2.5	3.0 ± 1.4	56.2 ± 17.1	24.9 ± 6.6	10.3 ± 3.0	6.4 ± 1.9	30.1 ± 7.1	5.1 ± 2.4	40.2 ± 9.6	45.2 ± 17.4	504 ± 50.1	41.1 ± 14.0	15.7 ± 3.0
	NiO-2	14.9 ± 3.3	5.9 ± 2.2	61.4 ± 26.7	19.6 ± 5.7	8.6 ± 1.8	7.6 ± 1.8	28.8 ± 4.7	4.8 ± 2.7	32.7 ± 8.5	40.1 ± 16.1	525 ± 36.6	29.8 ± 6.5	20.9 ± 8.9
	NiO-3	20.7 ± 5.2^	4.0 ± 2.1	66.6 ± 15.5	30.2 ± 6.9	6.7 ± 1.1	4.6 ± 1.1	29.0 ± 7.9	5.9 ± 1.0	28.9 ± 5.9	52.3 ± 14.0	539 ± 29.8	34.7 ± 10.0	14.4 ± 3.2
10d	DM	16.4 ± 2.4	2.3 ± 1.0	40.7 ± 14.1	25.6 ± 6.1	11.0 ± 2.9	10.5 ± 0.9	26.0 ± 3.4	5.4 ± 2.0	36.7 ± 4.2	45.6 ± 11.8	552 ± 28.5	26.8 ± 9.1	15.2 ± 3.4
	NiO-1	11.7 ± 2.0	3.9 ± 0.6	50.1 ± 16.1	24.7 ± 8.5	11.7 ± 3.2	11.7 ± 1.7	24.2 ± 4.5	4.7 ± 1.2	28.8 ± 7.0	46.7 ± 9.4	550 ± 37.2	30.7 ± 6.5	16.9 ± 2.1
	NiO-2	12.2 ± 2.5	1.7 ± 0.6	52.9 ± 14.2	22.3 ± 12.7	6.4 ± 2.7	6.1 ± 1.1	32.1 ± 6.6	6.0 ± 2.0	29.1 ± 8.0	61.2 ± 147	456 ± 49.6	28.6 ± 7.1	17.4 ± 2.2
	NiO-3	30.9 ± 5.7*	5.0 ± 0.5	53.4 ± 15.5	28.4 ± 10.7	8.2 ± 2.9	17.1 ± 3.0	31.7 ± 5.9	8.1 ± 3.1	30.7 ± 5.1	53.2 ± 20.1	439 ± 53.0	32.1 ± 4.7	22.1 ± 2.9
19d	DM	11.8 ± 1.5	2.3 ± 0.5	49.8 ± 14.7	22.7 ± 6.2	9.6 ± 4.1	10.2 ± 2.1	30.1 ± 5.0	3.1 ± 1.0	31.8 ± 5.0	55.8 ± 18.5	504 ± 31.1	35.5 ± 8.3	20.0 ± 2.7
	NiO-1	9.6 ± 2.2	2.2 ± 0.4	51.7 ± 15.4	23.8 ± 4.9	8.3 ± 2.8	6.2 ± 0.6	30.9 ± 8.7	2.9 ± 0.9	26.8 ± 4.5	49.6 ± 12.7	433 ± 55.4	41.2 ± 8.4	16.7 ± 2.5
	NiO-2	8.7 ± 0.8	2.0 ± 0.7	56.2 ± 12.0	22.1 ± 5.8	7.7 ± 2.9	5.7 ± 1.0	26.7 ± 6.4	5.5 ± 0.5	29.7 ± 3.7	48.8 ± 15.5	512 ± 65.6	40.3 ± 7.7	17.2 ± 4.8
	NiO-3	22.1 ± 0.7*	2.9 ± 0.6	39.6 ± 16.1	28.8 ± 4.7	11.2 ± 1.8	20.7 ± 1.9*	27.1 ± 4.9	4.7 ± 0.7	31.1 ± 3.6	53.2 ± 16.3	485 ± 20.0	33.9 ± 7.1	19.9 ± 4.6
29d	DM	8.7 ± 1.5	4.4 ± 0.9	55.2 ± 12.7	19.8 ± 3.0	10.3 ± 4.1	11.4 ± 2.3	25.7 ± 5.1	6.1 ± 0.5	30.6 ± 5.1	52.3 ± 15.7	487 ± 68.7	30.2 ± 10.5	16.0 ± 3.7
	NiO-1	7.6 ± 1.6	7.1 ± 2.0	67.1 ± 24.2	18.7 ± 6.9	5.5 ± 2.6	7.7 ± 2.6	29.9 ± 8.3	2.3 ± 0.5	26.5 ± 7.0	55.4 ± 14.5	463 ± 37.4	40.1 ± 6.1	14.3 ± 4.2
	NiO-2	9.3 ± 2.0	2.9 ± 1.0	43.2 ± 26.1	21.3 ± 5.8	7.8 ± 1.5	12.2 ± 2.1	33.7 ± 6.4	3.9 ± 1.1	32.7 ± 5.0	46.2 ± 13.2	503 ± 45.0	29.8 ± 5.2	21.1 ± 5.5
	NiO-3	12.7 ± 2.3	3.7 ± 1.7	55.5 ± 26.5	24.1 ± 4.2	9.1 ± 3.2	9.6 ± 0.9	31.0 ± 6.7	4.8 ± 1.0	27.1 ± 4.4	49.8 ± 18.8	522 ± 26.0	33.6 ± 8.8	18.1 ± 2.6
BALF														
1d	DM	2.3 ± 0.7	5.6 ± 3.2	14.2 ± 4.5	5.1 ± 3.6	0.9 ± 0.2	3.2 ± 0.3	2.4 ± 0.4	35.6 ± 11.4	88.8 ± 11.2	12.2 ± 1.9	25.2 ± 2.9	5.2 ± 1.0	21.0 ± 3.6
	NiO-1	2.0 ± 0.8	6.4 ± 2.3	18.7 ± 3.4	6.1 ± 2.9	1.0 ± 0.3	3.0 ± 0.4	3.6 ± 0.2	36.1 ± 9.9	90.5 ± 15.4	12.3 ± 2.3	30.2 ± 4.8	5.2 ± 1.0	20.9 ± 3.9
	NiO-2	2.1 ± 0.5	8.1 ± 3.8	15.2 ± 1.9	7.0 ± 2.0	1.2 ± 0.1	2.1 ± 0.5	3.4 ± 0.6	40.3 ± 6.9	101 ± 12.7	12.0 ± 3.2	25.7 ± 5.8	6.7 ± 1.0	22.1 ± 2.8
	NiO-3	3.1 ± 0.2	9.1 ± 4.7	20.1 ± 3.9	6.3 ± 1.9	1.3 ± 0.2	4.0 ± 1.2	3.7 ± 0.5	30.9 ± 5.9	108 ± 16.2	12.0 ± 4.0	22.3 ± 6.0	9.3 ± 2.0	22.3 ± 5.2
10d	DM	3.9 ± 0.9	4.4 ± 0.6	15.3 ± 4.5	6.7 ± 2.9	1.1 ± 0.2	4.1 ± 1.4	2.0 ± 0.2	30.3 ± 5.8	92.8 ± 15.4	12.0 ± 2.3	26.3 ± 5.5	6.3 ± 1.0	19.8 ± 3.4
	NiO-1	4.0 ± 0.6	6.5 ± 0.5	16.7 ± 2.9	5.2 ± 2.4	1.7 ± 0.1	5.1 ± 2.2	2.2 ± 0.1	29.2 ± 5.4	78.4 ± 16.2	12.7 ± 4.1	39.6 ± 3.9*	5.6 ± 0.7	28.7 ± 3.5+
	NiO-2	5.9 ± 1.5	5.0 ± 0.4	29.7 ± 3.4^	4.1 ± 2.9	3.8 ± 1.0	2.3 ± 1.3	2.9 ± 0.2	34.9 ± 6.0	77.9 ± 10.9	11.9 ± 2.9	31.4 ± 4.5	6.4 ± 1.5	20.6 ± 4.5
	NiO-3	16.2 ± 4.7*	10.1 ± 0.9*	22.7 ± 5.7	5.0 ± 3.7	2.1 ± 0.2	11.7 ± 3.9*	2.9 ± 0.2	31.8 ± 4.1	115 ± 9.5	10.9 ± 2.8	27.5 ± 8.8	15.5 ± 3.0*	24.3 ± 5.5
19d	DM	3.0 ± 1.0	2.1 ± 0.6	17.3 ± 4.2	5.1 ± 2.5	2.0 ± 0.3	5.0 ± 1.4	1.9 ± 0.3	34.8 ± 3.9	102 ± 8.5	10.8 ± 5.1	26.9 ± 9.5	5.9 ± 0.2	19.1 ± 2.8
	NiO-1	7.5 ± 3.1	5.4 ± 0.5	37.4 ± 5.8*	6.2 ± 2.9	1.3 ± 0.3	3.2 ± 0.5	2.0 ± 0.5	42.7 ± 8.2$	108 ± 11.4	21.1 ± 4.0*	24.7 ± 6.6	4.7 ± 1.4	24.8 ± 6.5
	NiO-2	9.7 ± 1.5#	4.8 ± 0.4	21.5 ± 3.2	5.1 ± 3.4	1.8 ± 0.4	2.9 ± 0.9	2.7 ± 0.2	55.1 ± 8.6$	170 ± 21.4+	11.6 ± 3.2	26.5 ± 5.2	6.5 ± 1.2	22.6 ± 4.4
	NiO-3	22.9 ± 4.2*	11.9 ± 0.9	18.7 ± 2.1	4.1 ± 2.7	5.2 ± 0.5*	12.0 ± 5.0*	3.8 ± 0.1	30.1 ± 9.1	96.4 ± 12.5	12.7 ± 2.0	25.0 ± 6.7	8.0 ± 3.3	23.0 ± 3.2
29d	DM	2.0 ± 0.3	5.2 ± 1.4	16.7 ± 3.4	4.8 ± 4.1	1.8 ± 0.2	4.0 ± 1.0	3.0 ± 1.0	29.8 ± 8.5	102 ± 14.0	12.1 ± 1.9	22.3 ± 5.2	4.3 ± 0.6	23.0 ± 3.4
	NiO-1	3.0 ± 0.2	6.7 ± 2.9	22.2 ± 2.5	5.4 ± 2.9	2.5 ± 0.6	2.5 ± 0.4	2.4 ± 0.6	33.3 ± 10.1	85.7 ± 16.5	10.8 ± 2.2	22.1 ± 3.2	4.1 ± 0.7	22.1 ± 5.5
	NiO-2	1.9 ± 0.6	5.9 ± 0.9	18.1 ± 1.2	6.2 ± 1.9	1.3 ± 0.5	6.1 ± 0.9	2.5 ± 0.5	34.0 ± 8.0	95.7 ± 18.5	11.5 ± 2.3	22.9 ± 3.6	4.9 ± 0.6	28.9 ± 2.2
	NiO-3	20.1 ± 5.6*	8.8 ± 0.8	21.1 ± 6.3	8.7 ± 3.0	3.8 ± 0.6+	10.2 ± 2.8*	4.0 ± 0.4	30.5 ± 5.9	94.7 ± 12.8	11.4 ± 3.7	23.8 ± 3.9	9.8 ± 2.4*	25.1 ± 3.1
					Th1/17 Cytokines					Th2 Cytokines			Other	

$n = 8$, $p < 0.05$.
*Statistical significance over all other groups at the corresponding time point.
#Statistical significance over DM.
°Statistical significance over DM, NiO-1.
+Significance over DM, NiO-2.
$Statistical significance over DM and NiO-3.

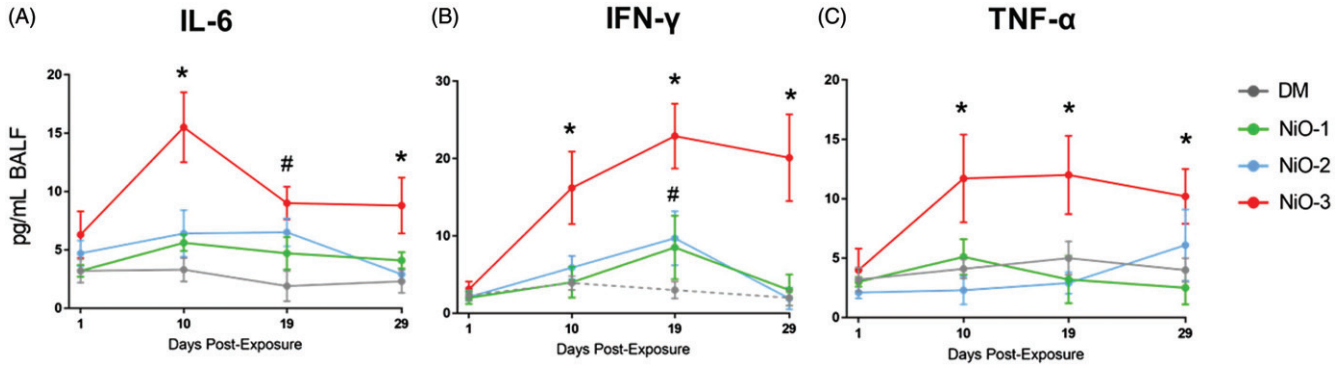

Figure 6. Levels of several notable Th1/pro-inflammatory cytokines that were elevated in the BALF of animals in the NiO time course study. BALF IL-6 (A), IFN-γ (B), and TNF-α (C) responses were generally conserved with respect to NiO surface area, wherein the higher dose (NiO-3) caused more pronounced and persistent increases. $n = 8$, $p < 0.05$, * indicates statistical significance over all other groups at the corresponding time point, # indicates statistical significance over DM only.

Table 4. Summary of histopathological findings from lungs of DM, NiO-1 (40 μg fine particle), and NiO-3 (40 μg ultrafine particle) groups at 1, 10, 19, and 29 d post-exposure in the NiO time course study.

		Accumulation alveolar macrophages	Black/brown particles in In alveolar macrophages	Infiltration mixed cell peribronchiolar/ perivascular	Edema peribronchiolar/ perivascular	Infiltration Neutrophil peribronchiolar/ perivascular	Exudate airways	Foreign material Airways	Hemorrhage
1d	DM	1,0,0,0,0,0	0,0,0,0,0,0	0,0,0,0,0,0	0,0,0,0,0,0	0,0,0,0,0,0	0,0,0,0,0,0	0,0,0,0,0,0	0,0,0,0,0,0
	NiO-1	1,0,0,0,0,0	1,1,1,1,1,1#	0,0,0,0,0,0	2,0,0,0,0,0	2,0,0,0,0,0	3,0,0,0,0,0	2,0,0,0,0,0	0,0,0,0,0,0
	NiO-3	0,0,0,0,0,0	1,1,1,1,1,1#	1,1,0,0,0,0	0,0,0,0,0,0	0,0,0,0,0,0	0,0,0,0,0,0	0,0,0,0,0,0	0,0,0,0,0,0
10d	DM	1,0,0,0,0,0	0,0,0,0,0,0	0,0,0,0,0,0	0,0,0,0,0,0	0,0,0,0,0,0	0,0,0,0,0,0	0,0,0,0,0,0	0,0,0,0,0,0
	NiO-1	0,0,0,0,0,0	1,1,1,1,1,1#	0,0,0,0,0,0	0,0,0,0,0,0	0,0,0,0,0,0	0,0,0,0,0,0	0,0,0,0,0,0	0,0,0,0,0,0
	NiO-3	1,1,1,0,0,0	1,1,1,1,1,1#	3,3,2,1,1,0*	1,0,0,0,0,0	0,0,0,0,0,0	0,0,0,0,0,0	0,0,0,0,0,0	0,0,0,0,0,0
19d	DM	0,0,0,0,0,0	0,0,0,0,0,0	0,0,0,0,0,0	0,0,0,0,0,0	0,0,0,0,0,0	0,0,0,0,0,0	0,0,0,0,0,0	0,0,0,0,0,0
	NiO-1	0,0,0,0,0,0	1,1,1,1,1,1#	0,0,0,0,0,0	0,0,0,0,0,0	0,0,0,0,0,0	0,0,0,0,0,0	0,0,0,0,0,0	0,0,0,0,0,0
	NiO-3	1,1,0,0,0,0	1,1,1,1,1,1#	2,2,2,1,1,1*	0,0,0,0,0,0	0,0,0,0,0,0	0,0,0,0,0,0	0,0,0,0,0,0	0,0,0,0,0,0
29d	DM	0,0,0,0,0,0	0,0,0,0,0,0	0,0,0,0,0,0	0,0,0,0,0,0	0,0,0,0,0,0	0,0,0,0,0,0	0,0,0,0,0,0	0,0,0,0,0,0
	NiO-1	0,0,0,0,0,0	1,1,1,1,1,1#	0,0,0,0,0,0	0,0,0,0,0,0	0,0,0,0,0,0	0,0,0,0,0,0	0,0,0,0,0,0	0,0,0,0,0,0
	NiO-3	1,0,0,0,0,0	1,1,1,1,1,1#	2,1,1,0,0,0*	1,0,0,0,0,0	0,0,0,0,0,0	0,0,0,0,0,0	0,0,0,0,0,0	2,0,0,0,0,0

Scores for each animal are compiled for each treatment group and histopathological finding. Scale: n = normal, 1 = minimal, 2 = mild, 3 = moderate, 4 = marked, 5 = severe. $n = 6$, $p < 0.05$.
#Statistical significance over DM at the corresponding time point.
*Significance over all groups.

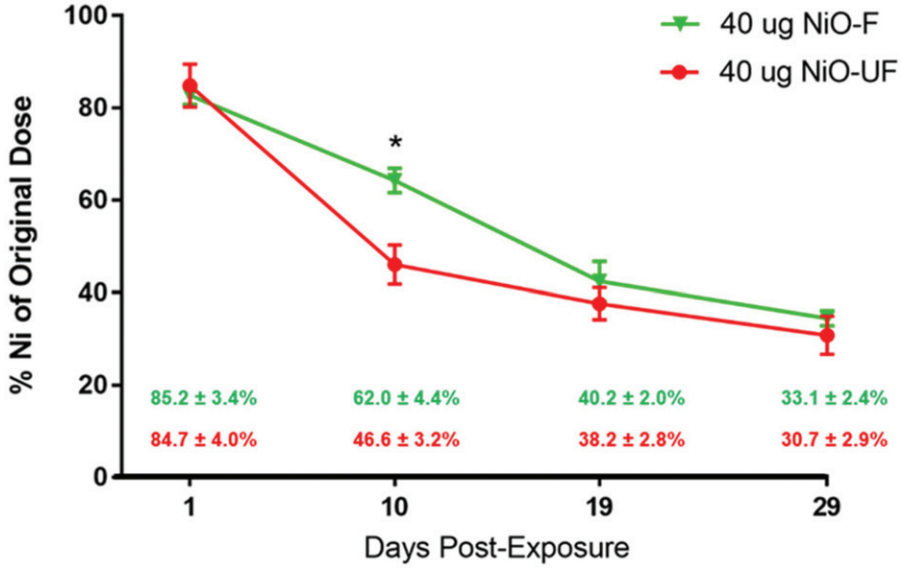

Figure 7. Whole lung nickel levels following aspiration of 40 μg the NiO-1 fine particle (green) or the NiO-3 ultrafine particle (red) in mice were measured by ICP-MS on dried lung tissue at 1, 10, 19, and 29 d post-exposure. Data is expressed as a percentage of the originally-administered dose. $n = 6$, $p < 0.05$, * indicates statistically significant difference between particles at the same time point.

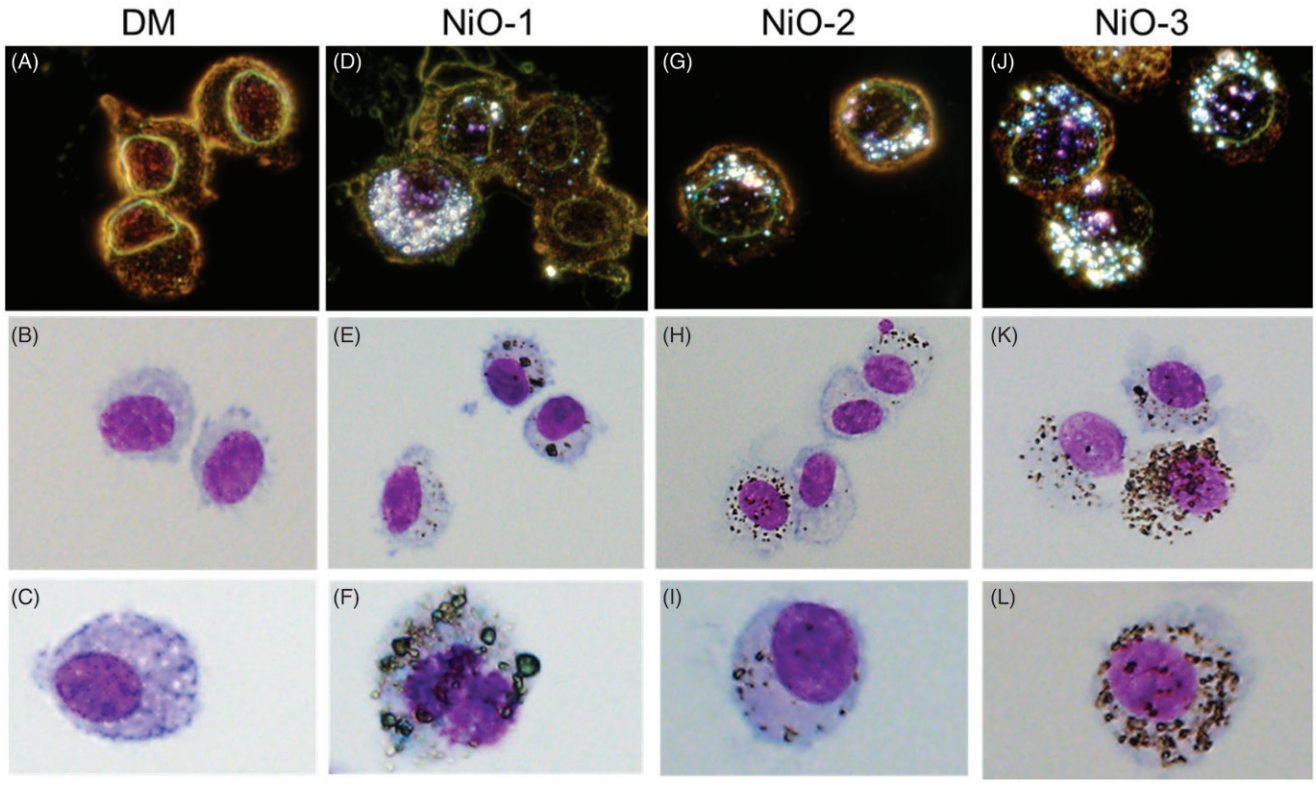

Figure 8. Dark field and light micrographs of alveolar macrophages recovered by BAL from each group at 10 d post-exposure. Images of macrophages isolated from the DM (A-C), NiO-1 (D-F), NiO-2 (G-I), and NiO-3 (J-L) groups showed variations in the degree of particle loading at 10 d, and size/morphology of internalized particles.

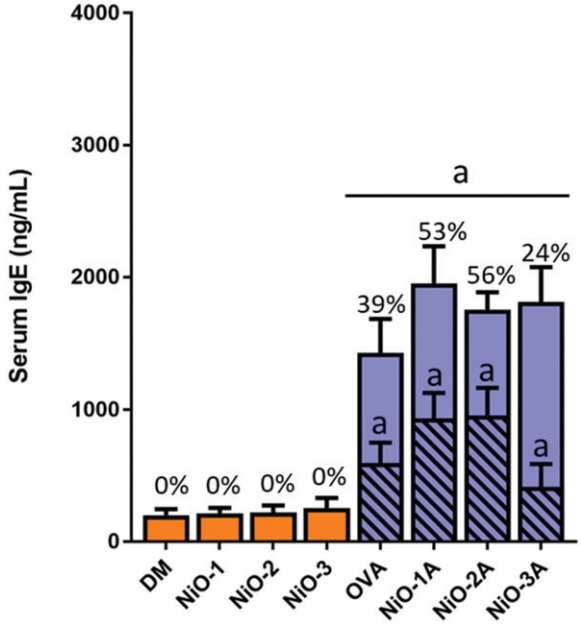

Figure 9. Levels of circulating total ($n = 3$–5) and OVA-specific ($n = 8$) IgE from serum of mice collected on day 14 of the OVA allergy model, following NiO aspiration and two sensitization procedures. Sensitized groups are shown in purple and non-sensitized groups are shown in orange. Total IgE levels are represented by the entire bar, OVA-specific IgE levels are represented by the hatched portion of the bar, and OVA-specific: total IgE ratio is expressed as a percentage over the corresponding bars. $p < 0.05$, "a" indicates statistically significant from all non-sensitized groups.

Day 28 post allergen-challenge lung function assessment

OVA-sensitized animals were challenged with OVA by aspiration on 19 d and 28 d, while control animals were aspirated with PBS. Directly following the second challenge on 28 d, mice were placed in whole body plethysmography chambers to monitor airway function, where P_{enh} values were recorded every 30 s for 6 h for each animal. A time course depiction of P_{enh} values for a single representative animal from DM, OVA, and all NiO-exposed/OVA sensitized groups is shown in Figure 10(A). Calculation of mean P_{enh} area under the curve (AUC) for each group showed a more robust pulmonary response to OVA challenge in the NiO-1 fine particle group, which was not present in either ultrafine particle group (Figure 10(B)). No differences in airway function were observed between the non-sensitized groups (data not shown).

Day 29 lung cellular influx and phenotyping

Mice were euthanized on 29 d and the lungs were lavaged to obtain cellular and fluid fractions for analysis. In the non-sensitized groups, there was an increase in total BAL cells in the NiO-3 compared to all other groups, which was consistent with findings from the time course study (Figure 11(A)). The total number of BAL cells was significantly increased in all OVA sensitized groups compared to non-

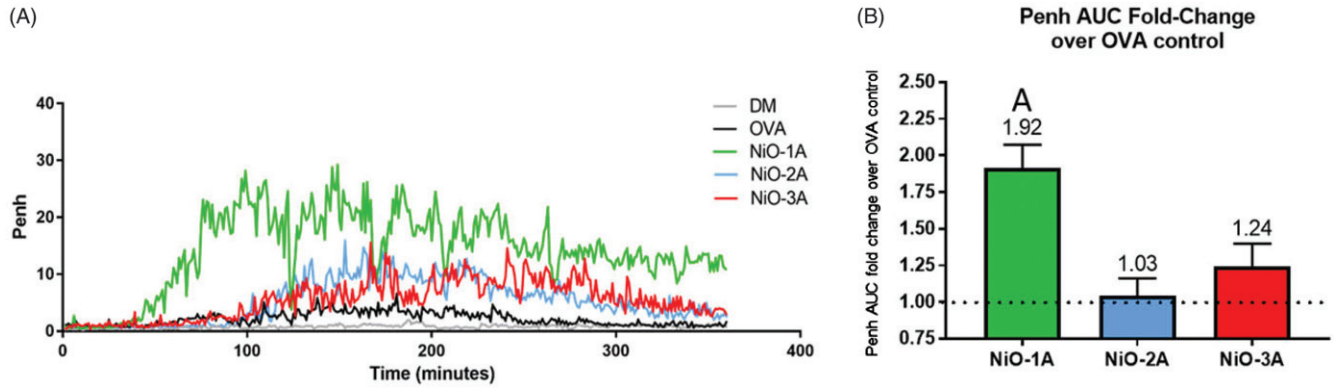

Figure 10. Whole body plethysmography results at day 28 of the OVA model. P_{enh} was recorded every 30 s for 6 h immediately following OVA aspiration challenge for each mouse. (A) A time course view of the P_{enh} response is shown for a single, representative animal from the DM, OVA, NiO-1A, NiO-2A, and NiO-3A groups. (B) Area under the curve was calculated, and averaged for animals from each group and expressed as fold-change over OVA control average. $n = 8$, $p < 0.05$, "A" indicates fold-change with statistical significance over all other groups.

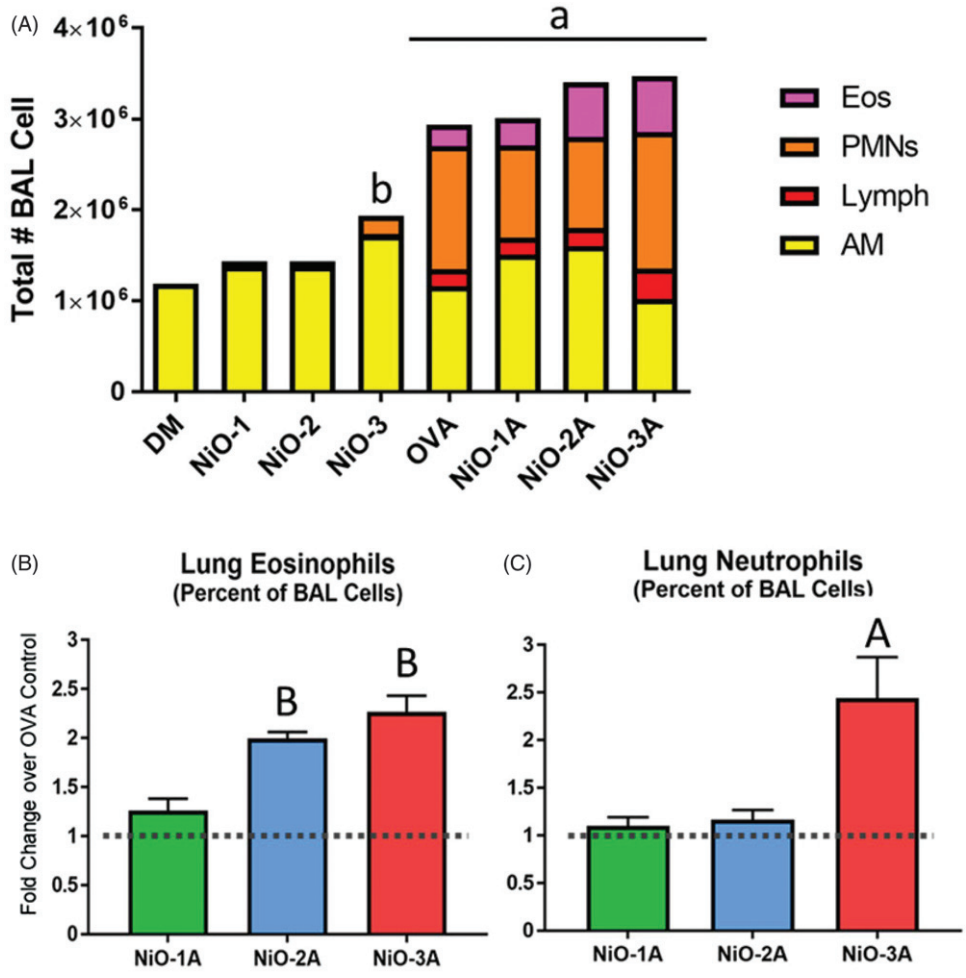

Figure 11. (A) Total cell number and fraction of eosinophils (pink), polymorphonuclear cells (orange), lymphocytes (red), and alveolar macrophages (yellow) recovered from BAL at day 29 in the OVA asthma model. $n = 8$, $p < 0.05$, "a" indicates total BAL cell number significant over all sensitized groups, "b" indicates significance over DM, NiO-1, and NiO-2. Percent eosinophils (B) and neutrophils (C) of total BAL cells are expressed as fold change over OVA control levels (dotted line). $n = 8$, $p < 0.05$. "A" indicates fold change significantly different from all other groups, "B" indicates fold change significantly different from NiO-1A.

sensitized groups, but no significant differences were observed between any sensitized groups. Phenotypical differentiation of BAL cells in the sensitized groups showed significant increases in percent lung eosinophils (Figure 11(B)) in groups exposed to NiO-UF (NiO-2A, NiO-3A), independent of dose mass or surface area. When compared to OVA control, percent lung neutrophils (Figure 11(C)) was similar between groups exposed to surface area-normalized doses (NiO-1A, NiO-2A). A significant increase in percent lung neutrophils was only observed in animals exposed to the highest NiO dose with respect to surface area, the NiO-3A group, when compared to OVA control.

(A)

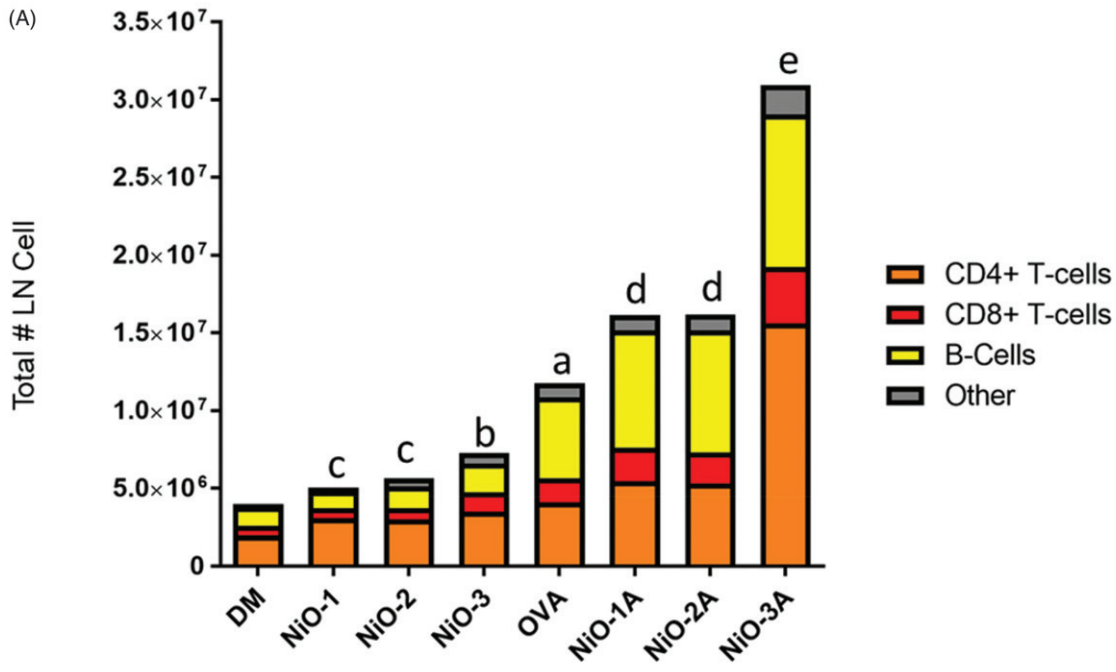

(B)

Day 29 NiO OVA Asthma Model
Lymph Node Cell Phenotypes by Percent of Total Cells

Group	Total LN Cells	CD4+ T-cells	CD8+ T-cells	B-cells	Other
DM	3,873,973 ± 499,632	55.2 ± 4.1%	14.2 ± 3.1%	26.1 ± 3.0%	4.5 ± 1.4%
NiO-1	5,856,315 ± 569,478 c	54.8 ± 3.0%	15.2 ± 2.3%	27.9 ± 2.9%	5.0 ± 1.0%
NiO-2	5,428,942 ± 442,989 c	55.9 ± 3.2%	13.7 ± 2.0%	30.2 ± 3.5%	6.3 ± 2.5%
NiO-3	7,552,486 ± 1,110,222 b	57.9 ± 2.9%	15.3 ± 2.8%	28.0 ± 2.5%	5.7 ± 2.4%
OVA	11,756,798 ± 1,420,407 a	36.8 ± 3.0% f	13.3 ± 1.9%	44.3 ± 4.0% f	5.6 ± 1.8%
NiO-1	16,192,731 ± 2,033,177 d	38.5 ± 2.9% f	15.1 ± 2.8%	45.0 ± 3.9% f	4.4 ± 0.8%
NiO-2	18,874,551 ± 1,956,100 d	35.9 ± 2.8% f	14.3 ± 2.7%	48.5 ± 5.0% f	6.3 ± 1.6%
NiO-3	30,939,970 ± 6,296,222 e	55.5 ± 4.1%	13.6 ± 1.7%	31.8 ± 4.2%	6.1 ± 1.4%

Figure 12. (A) Total number of cells (whole bar) and phenotypes [CD4+ T-cells (orange), CD8+ T-cells (red), and B-cells (yellow)] collected from the mediastinal lymph nodes at day 29 in the OVA asthma model. (B) The table shows the total cell number and percent of cell phenotypes in the OVA-exposed groups at day 29 depicted in the bar graph. $n = 8$, $p < 0.05$. "a" indicates statistical significance over all non-sensitized groups; "b" indicates statistical significance over DM, NiO-1, NiO-2; "c" indicates statistical significance over DM; "d" indicates statistical significance over all non-sensitized groups, OVA; "e" indicates statistical significance over all other groups; "f" indicates statistical significance over all non-sensitized groups, NiO-3A.

Day 29 lymph node and spleen cell phenotyping

Enumeration of mediastinal LN cells (Figure 12(A)) showed that all OVA-sensitized groups had elevated total LN cell numbers compared to non-sensitized groups. Among the NiO-exposed/OVA-sensitized animals, LN cell number in the NiO-3A group was significantly increased when compared to all other treatment groups. Phenotyping of LN cells (Figure 12(B)) showed consistent ratios of CD4+ T-cells, CD8+ T-cells, and B-cells between OVA, NiO-1A, and NiO-2A groups. However, in the NiO-3A group, the mediastinal LN contained a significantly increased proportion of CD4+ T-cells, and a significantly decreased proportion of B-cells compared to all other OVA-sensitized groups.

In the spleen, a similar trend was observed. OVA, NiO-1A, and NiO-2A groups all had similar proportions of CD4+ T-cells, CD8+ T-cells, and B-cells. In comparison, animals of the NiO-3A group had significantly lower percentages of B-cells and increased percentages of both CD4+ and CD8+ T-cells (data not shown).

Day 29 serum total and OVA-specific IgE levels

Total circulating IgE levels at 29 d were significantly increased in all OVA-sensitized groups (purple bars) compared to non-sensitized groups (orange bars), as shown in Figure 13. Moreover, all OVA-sensitized groups exposed to NiO, irrespective of particle size, dose mass, or dose surface area, had significantly increased total IgE levels when compared to OVA control levels. OVA-specific IgE levels, shown as the hatched area of the bars in Figure 13, were also quantified from serum and revealed no significant difference between the surface-area normalized groups (NiO-1A and NiO-2A) when compared to OVA control levels. Also, when compared to levels of serum total IgE, the proportion of OVA-specific IgE was similar between OVA control, NiO-1A, and NiO-2A groups, ranging from 56% to 63%. Contrarily, OVA-specific IgE levels in the NiO-3A group only comprised 19% of the total IgE and were significantly lower than the other NiO-exposed/OVA-sensitized groups.

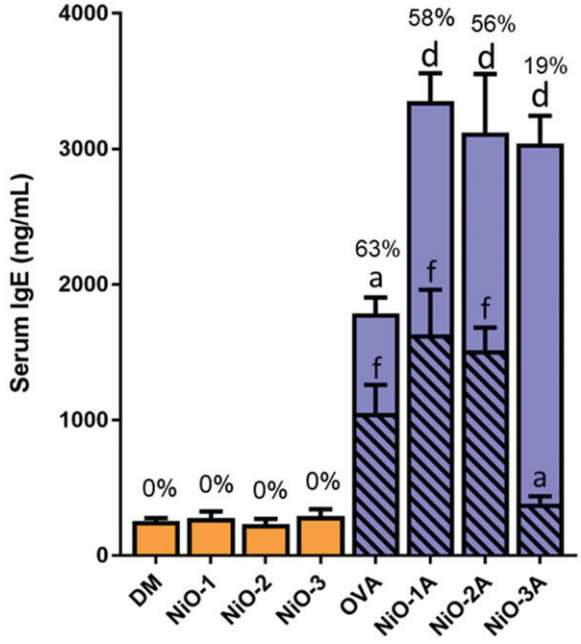

Figure 13. Levels of circulating total and OVA-specific IgE from serum of mice collected on day 29 of the OVA allergy model following NiO aspiration, two sensitization procedures, and two OVA challenges. Sensitized groups are shown in purple and non-sensitized groups are shown in orange. Total IgE levels are represented by the entire bar, OVA-specific IgE levels are represented by the hatched portion of the bar, and OVA-specific: total IgE ratio is expressed as a percentage over the corresponding bars. $n = 8$, $p < 0.05$. "a" indicates statistical significance over all non-sensitized groups; "d" indicates statistical significance over all non-sensitized groups, OVA; "f" indicates statistical significance over all non-sensitized groups, NiO-3A.

Day 29 BAL and serum cytokine analysis

Analysis of helper T-cell cytokine levels in BAL fluid showed that, when compared to OVA control levels, alterations in cytokine expression tended to be similar among groups exposed to equal doses of NiO with respect to surface area (Figure 14; Table 5). The NiO-1A and NiO-2A groups, which were exposed to NiO-F and NiO-UF, respectively, at equivalent surface areas of 192 mm^2 showed minimal changes in Th1/17 cytokine levels but robust increases in Th2 cytokines when compared to OVA control. Notably, IL-4 levels were increased over sixfold from OVA control and NiO-3A levels, consistent with these groups' elevated levels of OVA-specific IgE. Contrarily, animals of the NiO-3A group that were exposed to the higher ultrafine NiO surface area-based dose of 2580 mm^2 showed minimal increases in Th2 cytokines when compared to OVA controls. Rather, Th1/17 cytokines were significantly elevated when compared to NiO-1A, NiO-2A, and OVA control groups. While all NiO-treated OVA-sensitized groups had elevated IL-6 levels in the BAL fluid compared to OVA control animals, the degree of IL-6 increase appeared to be better correspond to NiO dose mass. Interestingly, the groups exposed to the higher mass of NiO (40 µg) had lower levels of BALF IL-6 compared to the group exposed to the lower 3 µg NiO-UF dose.

Serum cytokine levels demonstrated a similar trend between groups exposed to NiO doses with equivalent surface areas (Figure 15; Table 5). No clear trend was observed with respect to selective modulation of Th1/17 and Th2 cytokine levels in NiO-1A and NiO-2A groups; however, exposure to the higher NiO surface area (NiO-3A), resulted

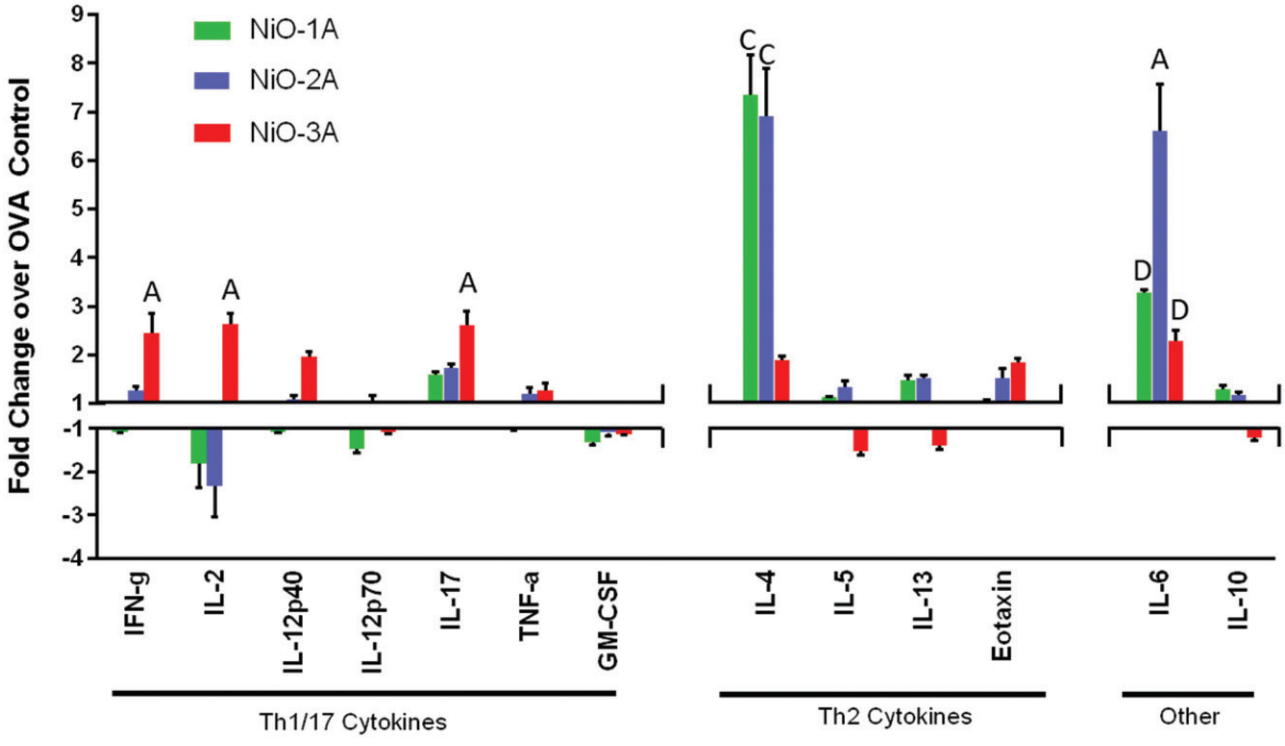

Figure 14. Th1/17 and Th2 cytokine levels in BAL fluid collected at day 29 from NiO-exposed/OVA-sensitized mice expressed as fold change over OVA control values. $n = 8$, $p < 0.05$. "A" indicates fold-change with statistical significance over all other groups; "C" indicates fold-change with statistical significance over OVA, NiO-3A; "D" indicates fold-change with statistical significance over OVA, NiO-2A.

Table 5. Raw values of serum and BALF cytokine levels for each treatment group at 29 d of the NiO OVA model.

	IFN-γ	IL-2	IL-12p40	IL-12p70	IL-17	TNF-α	GM-CSF	IL-4	IL-5	IL-13	Eotaxin	IL-6	IL-10
SERUM													
DM	12.9 ± 3.0	4.1 ± 2.1	42.2 ± 19.2	22.2 ± 4.0	12.2 ± 2.0	6.5 ± 2.0	33.1 ± 4.9	6.9 ± 2.4	32.4 ± 11.9	49.8 ± 12.1	464 ± 99.1	34.5 ± 6.8	17.6 ± 8.1
NiO-1	10.5 ± 3.1	3.7 ± 2.6	35.2 ± 14.5	26.8 ± 8.6	14.9 ± 1.6	8.8 ± 2.4	32.2 ± 10.2	4.8 ± 1.3	41.1 ± 12.0	52.5 ± 21.0	502 ± 93.2	30.7 ± 4.4	17.5 ± 5.1
NiO-2	13.8 ± 3.3	5.6 ± 1.6	35.7 ± 10.7	29.7 ± 6.2	9.9 ± 0.6	5.7 ± 2.9	28.0 ± 5.3	5.7 ± 1.4	39.1 ± 20.0	46.8 ± 19.7	498 ± 64.1	27.3 ± 5.4	18.5 ± 5.5
NiO-3	10.3 ± 2.3	4.2 ± 1.2	46.0 ± 13.7	30.1 ± 5.8	10.1 ± 2.8	10.0 ± 3.6	28.0 ± 6.6	4.0 ± 0.5	39.9 ± 13.1	49.0 ± 18.1	526 ± 82.4	29.6 ± 4.0	15.1 ± 6.6
OVA	14.7 ± 2.0	6.2 ± 1.7	109 ± 19.2[a]	66.5 ± 15.2[a]	13.7 ± 2.9	34.7 ± 3.9[a]	175 ± 15.1[a]	3.0 ± 2.0	206 ± 16.5[a]	553 ± 56.4[a]	1002 ± 100[a]	37.1 ± 6.7	112 ± 12.8[a]
NiO-1A	3.1 ± 0.5[d]	7.9 ± 1.8	109 ± 31.1[a]	160 ± 15.5[d]	18.8 ± 3.2	25.3 ± 5.4[a]	170 ± 14.7[a]	5.2 ± 1.7	214 ± 17.1[a]	518 ± 51.1[a]	989 ± 96.4[a]	39.1 ± 13.8	105 ± 11.2[a]
NiO-2A	10.0 ± 1.6	11.1 ± 3.0[a]	132 ± 41.0[a]	123 ± 17.6[c]	22.1 ± 3.6[e]	29.2 ± 4.5[a]	176 ± 16.6[a]	6.1 ± 1.7	220 ± 15.5[a]	596 ± 50.2[a]	896 ± 88.7[a]	47.1 ± 13.9	130 ± 18.4[a]
NiO-3A	23.4 ± 3.2[d]	18.7 ± 2.0[d]	230 ± 44.7[d]	98.7 ± 17.8[a]	16.6 ± 3.2	40.1 ± 6.4[f]	181 ± 15.4[a]	2.8 ± 1.1[g]	141 ± 18.0[d]	510 ± 44.7[a]	999 ± 102[a]	24.1 ± 5.6[h]	88.4 ± 9.1[a]
BALF													
DM	4.4 ± 1.0	5.6 ± 2.5	14.8 ± 3.6	9.7 ± 3.0	1.6 ± 0.5	4.2 ± 1.5	5.1 ± 1.1	33.3 ± 6.2	102 ± 19.8	13.4 ± 3.3	25.5 ± 3.0	3.5 ± 1.3	25.2 ± 5.0
NiO-1	2.7 ± 1.2	6.7 ± 1.8	15.5 ± 3.1	4.2 ± 2.0	1.4 ± 0.3	2.2 ± 1.1	3.2 ± 1.0	45.2 ± 10.4	99.8 ± 20.1	14.0 ± 4.2	24.5 ± 4.0	4.4 ± 1.2	21.0 ± 4.0
NiO-2	2.6 ± 0.9	10.1 ± 2.2	14.2 ± 2.0	6.5 ± 2.0	1.4 ± 0.7	4.8 ± 1.2	5.1 ± 2.2	33.2 ± 11.0	77.5 ± 15.2	12.5 ± 5.0	23.7 ± 6.9	6.5 ± 1.0	19.1 ± 3.3
NiO-3	12.2 ± 2.2[b]	11.0 ± 3.1	13.2 ± 4.9	7.1 ± 2.8	1.6 ± 0.5	11.1 ± 2.8[b]	4.2 ± 2.0	40.8 ± 9.8	105 ± 30.2	14.4 ± 3.2	22.1 ± 5.0	8.5 ± 3.7	18.2 ± 5.0
OVA	7.1 ± 3.1[b]	22.3 ± 5.3[a]	19.8 ± 4.5	4.7 ± 2.0	1.2 ± 0.4	17.0 ± 3.2[b]	10.1 ± 2.9[a]	78.4 ± 16.4[a]	472 ± 65.1[a]	25.5 ± 5.0[a]	70.9 ± 11.4[a]	58.9 ± 14.7[a]	41.4 ± 6.6[a]
NiO-1A	6.5 ± 1.0[a]	15.2 ± 4.8[i]	15.5 ± 4.2	3.5 ± 1.0	2.0 ± 0.5	15.4 ± 2.4[b]	8.2 ± 2.8[a]	572 ± 165[e]	512 ± 119[a]	32.7 ± 5.2[a]	74.9 ± 12.7[a]	111 ± 22.2[c]	44.0 ± 10.7[a]
NiO-2A	9.9 ± 2.1[b]	13.9 ± 3.1[j]	16.0 ± 4.0	5.2 ± 2.1	2.1 ± 0.5	16.2 ± 2.7[b]	9.1 ± 2.0[a]	568 ± 175[e]	501 ± 108[a]	29.1 ± 6.7[a]	80.1 ± 20.2[a]	356 ± 93.2[d]	45.1 ± 11.8[a]
NiO-3A	32.1 ± 8.1[d]	54.8 ± 8.1[d]	25.4 ± 6.7[a]	6.7 ± 2.8	5.5 ± 1.2[d]	18.8 ± 2.7[b]	6.3 ± 3.2	117 ± 19.2[c]	452 ± 123[a]	18.3 ± 4.1m	82.3 ± 38.1[a]	99.8 ± 20.7[c]	36.2 ± 7.7[a]
				Th1/17 Cytokines					Th2 Cytokines			Other	

$n = 8$, $p < 0.05$.
[a]Statistical significance over all non-sensitized groups.
[b]Statistical significance over DM, NiO-1, NiO-2.
[c]Statistical significance over all non-sensitized groups, OVA.
[d]Statistical significance over all other groups.
[e]Statistical significance over all non-sensitized groups, OVA, NiO-3A.
[f]Statistical significance over all non-sensitized groups, NiO-1A.
[g]Statistical significance over all non-sensitized groups, NiO-2A.
[h]Statistical significance over OVA, NiO-1A, NiO-2A.
[i]Statistical significance over DM, NiO-1.
[j]Statistical significance over DM, NiO-1, OVA.

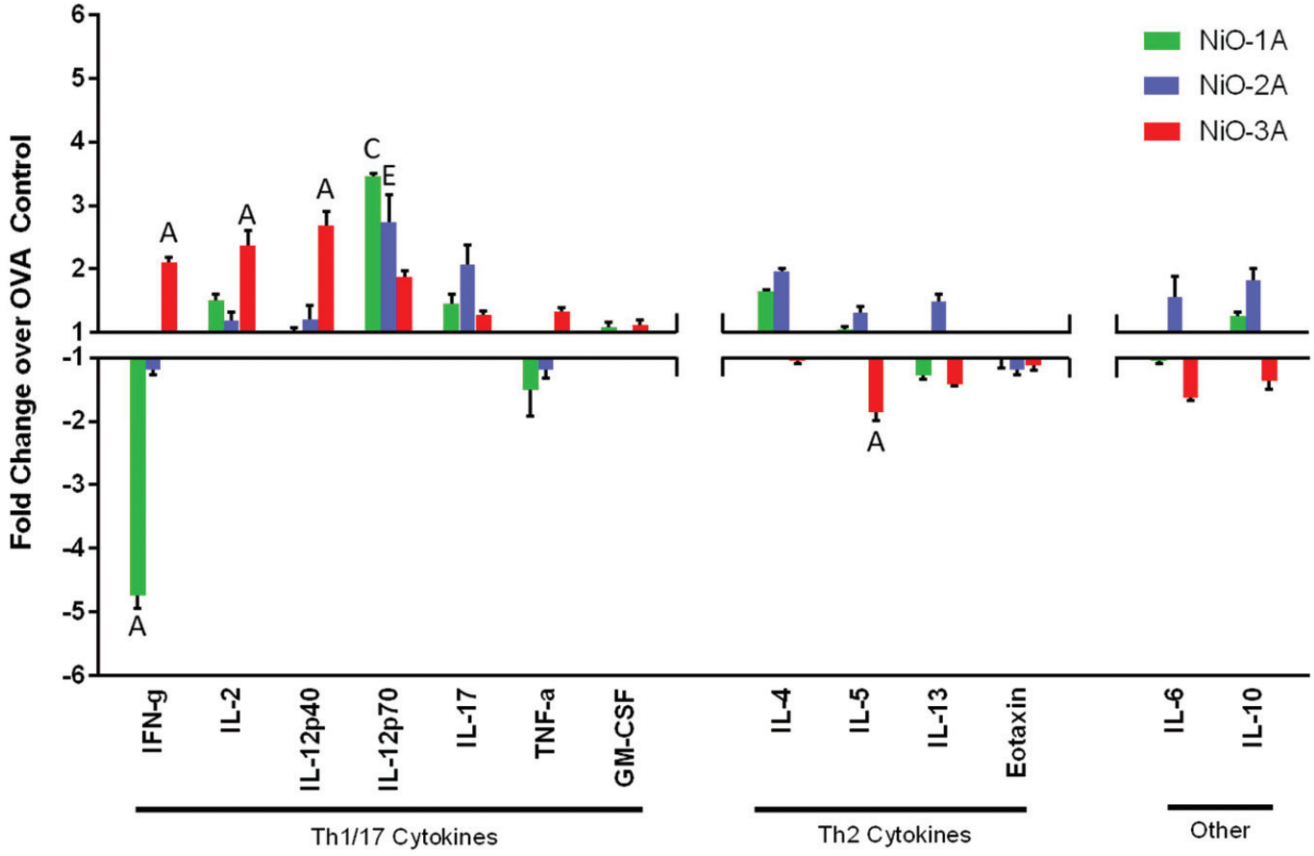

Figure 15. Th1/17 and Th2 cytokine levels in serum from NiO-exposed/OVA-sensitized mice expressed as fold change over OVA control values. $n = 8$, $p < 0.05$. "A" indicates fold-change with statistical significance over all other groups; "C" indicates fold-change with statistical significance over OVA, NiO-3A; "E" indicates fold-change with statistical significance over OVA.

in consistent elevations in Th1/17 cytokines and modest decreases in Th2 cytokines compared to OVA control levels-a similar pattern to that observed in the BAL fluid. Alterations in serum IFN-γ levels appeared unique to each group, as levels decreased over fivefold in the NiO-1A group, remained equal to OVA control levels in the NiO-2A group, and increased twofold in the NiO-3A group.

Day 29 lung tissue histopathological analysis

Lung tissue from all groups ($n = 6$) was collected for histological analysis of various parameters associated with respiratory allergy. The scores for each animal in each category of pathology are presented in Table 6. There were no notable observations made with respect to asthma-associated cellular or anatomical alterations in non-sensitized groups.

In sensitized animals, histopathological analysis reported inflammatory cell infiltration that was conducive with the differential phenotyping of inflammatory cells performed by flow cytometry. Macrophage accumulation and vacuolation was observed in all groups, and the degree of eosinophil and neutrophil influx varied between NiO-1A, NiO2-A, and NiO-3A groups, but corresponded with the findings generated by flow cytometry. Hypertrophy of the bronchial epithelium was observed in all groups, but most frequently observed in the NiO-3A group (80% incidence). Peribronchiolar edema and airway exudate was also observed in all sensitized groups, but no significant differences between treatment groups were noted. It was also noted that the presence of multinucleated giant cells was exclusively observed in the lungs of NiO-3A animals.

Discussion

The goal of these studies was to investigate the role of dose metrics in immune toxicity following pulmonary exposure to NiO particles of different sizes. Specifically, studies were designed to determine if exposure to NiO particles prior to sensitization and elicitation altered allergic responses. In the time course study, NiO-UF exposure was associated with a greater degree of lung injury and inflammation than NiO-F when administered in equal mass doses (NiO-3 vs NiO-1). When NiO-UF was administered in a dose normalized for the surface area of the NiO-F dose (NiO-2), this discrepancy was mitigated. Contrarily, in the OVA asthma model, immune endpoints related to the allergic response were differentially impacted by multiple NiO-F and NiO-UF dose metrics. NiO exposure, irrespective of any metric, resulted in elevated circulating total IgE levels at 29 d. Exposure to surface area-normalized doses (NiO-1A and NiO-2A) resulted in similar responses with respect to OVA-specific IgE levels, BALF/serum cytokines, and lung neutrophils. However, lung eosinophil and P_{enh} response appeared better correlated to particle size with NiO-F (NiO-1A) exposure

Table 6. Summary of histopathological findings from lungs of all groups at day 29 in the NiO OVA model.

	Accumulation alveolar macrophages	Infiltration eosinophil, mononuclear peribronchiolar/ perivascular	Infiltration mixed cell peribronchiolar/ perivascular	Black/brown particles in In alveolar macrophages	Accumulation Macrophages, eosinophil, neutrophil in alveolar lumens	Bronchiole epithelium hypertrophy	Multi-nucleated giant cells	Macrophage vacuolation	Edema peribronchiolar/ perivascular	Exudate airways	Macrophages, neutrophils at terminal bronchiole/ alveolar duct	Hemorrhage
DM	0,0,0,0,0,0	0,0,0,0,0,0	0,0,0,0,0,0	0,0,0,0,0,0	0,0,0,0,0,0	0,0,0,0,0,0	0,0,0,0,0,0	0,0,0,0,0,0	0,0,0,0,0,0	0,0,0,0,0,0	0,0,0,0,0,0	0,0,0,0,0,0
NiO-1	1,1,0,0,0,0	0,0,0,0,0,0	1,1,0,0,0,0	1,1,1,1,1,1[a]	0,0,0,0,0,0	0,0,0,0,0,0	0,0,0,0,0,0	0,0,0,0,0,0	0,0,0,0,0,0	0,0,0,0,0,0	1,0,0,0,0,0	0,0,0,0,0,0
NiO-2	1,0,0,0,0,0	0,0,0,0,0,0	0,0,0,0,0,0	1,1,1,1,1,1[a]	0,0,0,0,0,0	0,0,0,0,0,0	0,0,0,0,0,0	0,0,0,0,0,0	0,0,0,0,0,0	0,0,0,0,0,0	0,0,0,0,0,0	1,0,0,0,0,0
NiO-3	1,0,0,0,0,0	0,0,0,0,0,0	1,1,1,1,1,0[b]	1,1,1,1,1,1[a]	0,0,0,0,0,0	0,0,0,0,0,0	0,0,0,0,0,0	1,0,0,0,0,0	0,0,0,0,0,0	0,0,0,0,0,0	0,0,0,0,0,0	0,0,0,0,0,0
OVA	0,0,0,0,0,0	2,2,2,2,2,2[c]	0,0,0,0,0,0	1,1,1,1,1,1[a]	1,1,1,1,1,1[c]	1,1,1,1,1,1[c]	0,0,0,0,0,0	1,1,1,1,1,1[c]	0,0,0,0,0,0	1,0,0,0,0,0	0,0,0,0,0,0	0,0,0,0,0,0
NiO-1A	0,0,0,0,0,0	2,2,2,2,2,1[c]	0,0,0,0,0,0	1,1,1,1,1,1[a]	2,1,1,1,1,1[c]	1,1,1,1,1,0[c]	0,0,0,0,0,0	1,1,1,1,1,1[c]	1,1,0,0,0,0	1,1,0,0,0,0	0,0,0,0,0,0	0,0,0,0,0,0
NiO-2A	0,0,0,0,0,0	2,2,2,2,2,2[c]	0,0,0,0,0,0	1,1,1,1,1,1[a]	1,1,1,1,1,1[c]	1,1,1,1,1,0[c]	0,0,0,0,0,0	1,1,1,1,1,0[c]	1,1,0,0,0,0	1,0,0,0,0,0	0,0,0,0,0,0	0,0,0,0,0,0
NiO-3A	0,0,0,0,0,0	3,2,2,2,2,1[c]	0,0,0,0,0,0	1,1,1,1,1,1[a]	2,1,1,1,1,0[c]	1,1,1,1,1,0[c]	1,1,0,0,0,0	1,1,1,1,1,1[c]	1,1,1,0,0,0	1,1,0,0,0,0	0,0,0,0,0,0	0,0,0,0,0,0

Scores for each animal are compiled for each treatment group and histopathological finding and compared to corresponding control (DM for non-sensitized groups, OVA for sensitized groups). Scale: n = normal, 1 = minimal, 2 = mild, 3 = moderate, 4 = marked, 5 = severe. $n = 6$, $p < 0.05$.

[a]Difference over DM.

[b]Statistical significance over DM, NiO-1, NiO-2.

[c]Statistical significance over all non-sensitized groups.

resulting in greater airway reactivity (increased P_{enh}) and NiO-UF (NiO-2A and NiO-3A) resulting in increased lung eosinophil burden.

The nature of NiO-induced pulmonary inflammation and the kinetics of resolution observed in the NiO time course study are consistent with other studies that have investigated NiO nanoparticle-induced acute lung inflammation *in vivo* (Ogami et al. 2009a, 2009b; Horie et al. 2011, 2012; Bai et al. 2018). Some metal nanomaterials have been associated with the induction of eosinophil-dominant inflammation in the lung, but the neutrophilic-dominant inflammation observed following NiO exposure in this study (Figure 4(C)) is in agreement with other existing investigations of NiO nanoparticles (Cho et al. 2010; Morimoto et al. 2010, 2011; Mizuguchi et al. 2013; Cao et al. 2016; Jeong et al. 2016a). The magnitude of lung injury and inflammation caused by NiO was correlated to surface area of the administered particles in this study; the ultrafine particle at the high dose (the highest surface area and the greater number of particles per mass) caused the greatest degree of injury and inflammation (Figure 4), followed by the fine particle at the high dose and the ultrafine particle at an equivalent surface area-based dose, particularly at 10 d post-exposure.

Although dose metrics including particle number and particle volume have been occasionally cited as parameters predictive of the toxic potential of some meal nanomaterials, a similar association between lung inflammation and NiO surface area has been previously reported in other studies (Ingham and Fisher 2000; Zhang et al. 2003; Poland et al. 2012; VanOs et al. 2014; Sager et al. 2016a; Lehmann et al. 2018). Surface area has also been reported to be the dose parameter that best represents the magnitude of acute pulmonary toxicity induced by other metal-based nanomaterials including titanium dioxide (TiO_2NP) and various carbon-based materials (Stoeger et al. 2006; Sager et al. 2008; Hussain et al. 2009; Sager and Castranova 2009; Schmid and Stoeger 2016). Contrarily, dose mass has been shown to better predict the severity of lung injury caused by other metal-based nanoparticles including zinc oxide (ZnONP), cobalt oxide (CoONP), and copper oxide (CuONP) (Ho et al. 2011; Jeong et al. 2016b).

Inconsistencies between the dose metric best correlated to the toxic potential of different metal nanomaterials often reflect variations in their mechanisms of toxicity. For example, particle number has been largely implicated as a parameter best correlated to the toxic potential of nanomaterials exhibiting long, fiber-like morphologies. Rigid nanofibers and nanowires with high aspect ratios are often associated with the induction of frustrated phagocytosis, compromised locomotion, and or death of alveolar macrophages following pulmonary exposure. Since a single nanofiber has the potential to trigger the release of pro-inflammatory cytokines and damage-associated molecular patterns (DAMP) by an individual macrophage and compromise clearance of foreign material from the airways, particle number often reflects the magnitude of pulmonary inflammation caused by nanofibers and nanowires with high aspect ratios (Poland et al. 2012; Schinwald et al. 2012;

Schinwald and Donaldson 2012). Comparatively, dose mass has been frequently implicated in the toxic potential of metal nanomaterials with high dissolution potential, such as ZnONP, CoONP, CuONP. These particles often induce toxic effects resulting from the rapid release of cytotoxic metal ions from the parent particle. Likewise, the absolute quantity of ions capable of being released from these nanomaterials is related to the mass of the administered dose, rendering it a dose metric correlated to the degree of toxicity driven by this mechanism (Jeong et al. 2016b). Contrarily, NiO nanoparticles and other metal nanomaterials known to be relatively insoluble at neutral pH are frequently associated with toxic effects that emerge as a result of particle surface-interactions. Subsequent ROS formation, oxidative stress, and perturbation of cellular structures have been cited as mechanisms involved in their acute toxic effects on the lungs (Schmid and Stoeger 2016). Accordingly, the surface area of the administered dose better represents the magnitude of resultant tissue injury. Moreover, additional physico-chemical characteristics with implications for surface area-dependent toxic effects have also been implicated in the toxic response. NiO nanoparticle pre-exposure dispersion state, surface modification, and morphology have all been shown to influence the inflammatory response caused by NiO nanomaterials in the lungs (Poland et al. 2012; Sager et al. 2016a, 2016b; Mo et al. 2019). These findings also emphasize important considerations for dosimetrics, highlighting the potential relevance of dose parameters such as surface chemistry and particle number on a mass basis, which may be increasingly relevant in future studies (Mo et al. 2019).

The only marker throughout the time course study that differed between treatment groups exposed to NiO surface area-normalized doses (NiO-1 and NiO-2) was the mediastinal LN size at 29 d (Figure 5). The kinetics and degree of LN expansion were similar between the NiO-1 and NiO-2 groups until the 29 d time point, when the LN size of the NiO-2 group continued to increase, reaching values equivalent to that of the NiO-3 group at the same time point. Contrarily, LN size at 29 d in the NiO-1 group had decreased from the response recorded at 19 d; however, it remained significantly elevated compared to corresponding control levels. Likewise, each group exhibited unique responses in the LN during the time course that differed with respect to the kinetics of size increase and magnitude of this response. Several contributing factors may be responsible for this observation, including NiO dissolution kinetics and particle deposition/clearance patterns in relationship to immune cell signaling.

Increased LN cellularity may reflect expansion of lymphocyte populations in response to local immune activation driven by the release of Ni ions. Both NiO particles were relatively insoluble at neutral pH, but their dissolution was shown to be accelerated in acidic environments, as demonstrated in the ALF (Figure 3), which represents the environment encountered by particles following uptake by pulmonary phagocytes. Subsequent dissolution of particles and release of toxic ions can result in pro-inflammatory signaling by macrophages, as well as necrotic cell death, leading to the release of DAMP and cytotoxic ions into the airways. All of these effects can trigger inflammatory reactions leading to proliferation of lymphocyte populations in the lung-draining LN. In this study, *ex vivo* analysis showed that dissolution was similar for NiO-UF and NiO-F in the acidic ALF solution, making it difficult to attribute differences in dissolution rate to the variations in LN size increase between the NiO-1 and NiO-2 groups at 29 d. However, it is important to note that while *ex vivo* analysis did not reveal differences in dissolution behavior between NiO-F and NiO-UF, this approach cannot account for the numerous complexities of the *in vivo* environment that can impact particle dissolution. Moreover, numerous particle-independent factors could have contributed to differences in the rate of ion release from the surface area-normalized doses of NiO-F and NiO-UF *in vivo*. For example, an increased number of alveolar macrophages in the lungs of one group could have resulted in enhanced particle dissolution; however, at the time points investigated in this study, cellular recruitment to the lungs did not differ between the NiO-1 and NiO-2 groups. Overall, it remains unclear if the differences in LN size increase between these groups were reflective of differences in the rate of ion release between particles.

Comparatively, the increase in LN size may reflect the translocation of pulmonary immune cells to the LN. Accordingly, the early LN expansion characteristic of the NiO-3 group (Figure 5) may have been correlated to the pulmonary clearance kinetics of the ultrafine particles versus the fine particles with respect to dose mass (Figure 6). Following exposure to a 40 µg dose of either particle, 47% of the original Ni dose remained in the lungs of the NiO-3 group at 10 d, versus 62% in the NiO-1 group. However, by 29 d, lung Ni burden was similar between groups. Size-specific particle deposition patterns in the alveolar region and airways may have contributed to differences in the rate of cell-mediated particle clearance with respect to mass. Deposition of particles in different anatomical compartments of the respiratory tract can lead to differences in the propensity for local retention of particles in the lung parenchyma, their likelihood for uptake by pulmonary phagocytes, potential for cell-mediated transport via lymphatics, or physical translocation by the mucociliary escalator (Bezemer 2009). These factors can all impact the quantity of particles that translocate to the LN, as well as their kinetics of relocation. Many other features of the administered dose may also impact these processes. For example, dose volume is known to contribute greatly to the overloading of pulmonary phagocytes, which can trigger alterations in cell migratory potential (Oberdorster et al. 1992). Particle number, dose mass, and surface area can also impact macrophage responses with potential to modulate the clearance of particles. In this study, it is difficult to discern the material properties and factors that account for the differences in temporal patterns of lymphocyte expansion between groups. Likewise, the time-dependent increase in LN size following NiO exposure may reflect discrepancies in the absolute quantity and time course of ion release, as well as

deposition and clearance patterns of the delivered dose as a function of particle size, mass, and/or surface area.

Although numerous studies have been conducted to help elucidate the role of various nanomaterial physico-chemical properties on lung toxicity, there are considerably fewer studies that examine the potential for metal nanomaterial exposure to augment immunological processes in allergy models; moreover, even fewer studies have examined the role of nanomaterial characteristics and dose metrics on this immunomodulatory potential. Incorporation of the NiO-F and NiO-UF particles into the OVA study demonstrated that, contrary to the surface area-dependent general pulmonary inflammation caused by NiO, multiple dose metrics impacted immune endpoints with implications for asthmatic responses.

In the OVA model, the pulmonary response to allergen challenge and number of lung eosinophils were both parameters that appeared associated with NiO particle size. Increases in lung eosinophils and enhanced bronchoconstrictive responses are two features of allergic airway disease that generally present simultaneously in asthma, wherein the extent of their involvement is frequently correlated to clinical disease severity (Cockcroft and Davis 2006). Interestingly, these responses were differentially increased as a function of NiO particle size in the OVA model. NiO-F exposure was associated with enhanced P_{enh} responses compared to OVA controls (Figure 10), whereas increased lung eosinophil recruitment occurred in response to NiO-UF exposure (Figure 11(B)). Furthermore, the groups demonstrating the most robust P_{enh} and eosinophil responses in this study did not exhibit the most pronounced responses with respect to other prototypical markers of allergic reactivity, including OVA-specific IgE and Th2 cytokine levels.

Average P_{enh} values were only elevated in the NiO-1A group, the only group exposed to NiO-F. As a parameter indicative of resistance to airflow, alterations in P_{enh} may result from several different underlying mechanisms. Non-immunological mechanisms capable of increasing resistance to airflow include exposure-induced structural or physiological alterations that impact the mechanics of respiration. For example, modulation of airway smooth muscle signaling and subsequent contractility behavior has been demonstrated following exposure to several metal nanomaterials (Gonzalez et al. 2011; Kapilevich et al. 2012; Lin et al. 2018). However, no P_{enh} alterations were observed in non-sensitized groups exposed to NiO, suggesting that the P_{enh} response observed in the NiO-1A group was both particle-specific and dependent on an immunologically-based mechanism associated with the asthmatic condition.

The enhanced P_{enh} response selectively observed in animals exposed to the larger NiO particle may reflect interference with bronchoconstrictive responses resulting from interactions between NiO particles and various molecular mediators of asthmatic elicitation. Microscopic analysis of lung tissue and cells in the lavage fluid revealed that NiO particles were still abundantly present in the airways and pulmonary phagocytes at 29 d. The presence of these particles during allergen challenge can have notable implications for allergic processes since protein allergens, immunoglobulins, chemokines, and cytokines have all been shown to exhibit altered biological activity upon interaction with metal nanomaterials (Brown et al. 2010; Radauer-Preiml et al. 2016). Notably, granulocytes and IgE molecules, when pre-exposed to nanoparticles, have been shown to exhibit compromised binding activity, preventing cellular degranulation (Ortega et al. 2015). Likewise, alterations in P_{enh} reactivity and other markers of elicitation response severity in the OVA model may have been subject to influence from persistent NiO particle presence in the airways. The extent of such effects would be dependent on the burden of NiO particles remaining in the respiratory tract (dose-dependent clearance of particles), number of particles free from cellular- or tissue-mediated immobilization, and properties associated with the surface-loading capacity of particles, such as surface area.

The degree of eosinophil influx to the lungs was another marker in the OVA model that correlated with particle size. However, contrary to the enhanced P_{enh} reaction, which was exclusively associated with exposure to the larger particle, increased eosinophil recruitment was associated with exposure to the smaller NiO particle (at both doses). One of the major cytokines responsible for recruitment of eosinophils to the lungs is IL-5, a prototypical Th2 cytokine (Rankin et al. 2000). However, neither group with elevated numbers of lung eosinophils (NiO-2A, NiO-3A) exhibited significant elevations in BALF IL-5 levels (Figure 14). This observation suggests that non-immunological mechanisms may be responsible for the increase in eosinophil recruitment in these groups. In this regard, NiO nanoparticles have been shown to recruit eosinophils to the lungs *in vivo* as a result of their internalization by cells, where accumulation in acidic lysosomes facilitates the release of cytotoxic ions, causing necrotic cell death. Eotaxin is passively released by these dying cells, triggering the local influx of eosinophils, independent of IgE-mediated or Th2-biased mechanisms (Lee et al. 2016).

Several studies have shown that the rate of ion release from metal nanomaterials is a critical determinant in the selective recruitment of neutrophils and eosinophils to the airways. Generally, insoluble and highly soluble metal nanomaterials have been associated with the preferential induction of neutrophilic- and eosinophilic-dominant inflammation, respectively (Cho et al. 2010; 2012b). A study by Jeong et al. (2015) illustrates this concept. In the study, cobalt nanoparticles with divergent solubility profiles were instilled into the lungs of rats, and the subsequent inflammatory responses were characterized. The insoluble Co_3O_4 nanoparticles produced neutrophilic-driven inflammation, whereas the soluble CoO nanoparticles induced eosinophilic-dominant inflammation. Moreover, the number of neutrophils recruited to the lung was strongly correlated to the surface area of the administered Co_3O_4 dose. Comparatively, the number of eosinophils recruited to the airways by CoO strongly correlated with the dose of cobalt ions released from the parent particles, and mirrored the

inflammatory profile caused by the highly soluble salt, $CoCl_2$ salts (Jeong et al. 2015).

Collectively, these observations suggest that the influx of phenotypically-distinct inflammatory cell populations in healthy and allergic airways following NiO exposure may be associated with differences in particle dissolution potential as a result of disease state-specific microenvironments. The exclusive recruitment of neutrophils to the lungs of animals in the NiO time course study and non-sensitized groups of the OVA model are consistent with the insoluble nature of NiO-F and NiO-UF in neutral conditions. By comparison, the recruitment of eosinophils exclusively observed in the NiO-2A and NiO-3A groups of the OVA model suggests that the present of established allergic airway inflammation enhanced the dissolution potential of NiO-UF. In this study, although analysis of particle dissolution *ex vivo* showed that NiO-UF and NiO-F did not differ significantly in acidic conditions over time (Figure 3), NiO-UF showed a trend for a higher degree of dissolution than NiO-F. This effect may be exacerbated *in vivo* due to the increased complexity of the environment in the phagolysosme, as well as potentially the increased acidic environment of asthmatic airways (Hunt et al. 2000). Further studies are necessary to better discern the role of particle solubility in relation to the particle size-specific inflammatory response caused by NiO in allergic disease.

The inverse relationship between enhanced P_{enh} reactivity and eosinophil lung burden in the OVA model is a nonconventional finding. However, several potential mechanisms may be responsible for this effect. For example, the release of toxic granule proteins by eosinophils has the potential to cause significant injury to lung tissue, which can alter airflow mechanics and mask bronchoconstrictive responses measured by whole body plethysmography. This effect could explain the increases in lung eosinophil burden observed in the NiO-2A and NiO3-A group, despite the absence of enhanced P_{enh} responses. Similarly, since eosinophils can modulate neural communication with airway smooth muscle cells, an increased lung eosinophil burden might be responsible for interference with signaling pathways involved in allergen-induced bronchoconstriction (Kato et al. 2006). Furthermore, since eosinophils have the capacity to bind IgE molecules, increased numbers of lung eosinophils may have led to immobilization of allergen or other molecular mediators involved in triggering or amplifying P_{enh} responses (McBrien and Menzies-Gow 2017).

Another interesting observation in the OVA model was the impact of NiO exposure on immunoglobulin production and specificity. At 29 d, levels of total IgE were elevated in all NiO-exposed/OVA-sensitized groups, irrespective of NiO particle size, mass, or surface area (Figure 13). Comparatively, OVA-specific IgE levels were conserved between groups with respect to NiO surface area. Although exposure to the smaller of the two surface area-based doses (NiO-1A and NiO-2A groups) was associated with a minor increase compared to OVA controls, the effect was not statistically significant. Contrarily, exposure to the larger surface area-based dose (NiO-3A group) was associated with a significant decrease in OVA-specific IgE production compared to all other sensitized groups. This discord between NiO dose/exposure effects on total and OVA-specific IgE levels at 29 d resulted in a notable discrepancy in the IgE specificity ratio between groups. The NiO-1A and NiO-2A groups exhibited a similar IgE profile as OVA controls, wherein OVA-specific IgE constituted 58%, 56%, and 63% of all IgE, respectively. By comparison, allergen nonspecific IgE dominated the IgE repertoire of the NiO-3A group, as only 19% of the total circulating IgE was OVA-specific.

Although NiO dose-dependent alterations in the IgE repertoire were observed at 29 d, this response could be indicative of NiO adjuvant activity during OVA sensitization or particle-induced modulation of the elicitation response. Therefore, IgE levels were also assessed at 14 d in order to clarify if NiO exposure was capable of inducing sensitization-specific effects, independent of allergen challenge. No differences in the levels of total or OVA-specific IgE were observed between NiO-exposed/OVA-sensitized groups at 14 d (Figure 9). However, differences in the proportionality of IgE specificity were discernable between groups at 14 d. In OVA control animals, OVA-specific IgE comprised 39% of the total IgE pool after sensitization. Comparatively, OVA-specific IgE constituted 53%, 56%, and 24% of the total IgE in the NiO-1A, NiO-2A, and NiO-3A groups, respectively. Since antibody production, irrespective of allergen specificity, did not differ between groups with respect to quantity, this finding implies that pulmonary NiO exposure did not compromise the capacity for B-cells to undergo isotype switching in response to systemic sensitization. However, the existence of differences in the proportionality of IgE specificity between groups suggests that respiratory NiO exposure can compromise other peripheral immune processes, such as somatic hypermutation and affinity maturation in B-cells.

In this study, NiO exposure prior to allergic sensitization was associated with a modest impact on antibody production during allergic sensitization, as illustrated by the similar IgE levels between groups at 14 d. By comparison, many other studies using allergy models have demonstrated that exposure to metal nanomaterials during the sensitization phase of allergy can cause profound adjuvant effects. TiO_2NP, ZnONP, SiO_2NP, and aluminum nanoparticles (AlNP) have all been shown to induce prominent increases in antigen-specific antibody levels following both systemic and mucosal sensitization, independent of allergen challenge (de Haar et al. 2006; Yoshida et al. 2011; Li et al. 2014; Roy et al. 2014; Toda and Yoshino 2016). However, a key discriminating feature between these studies and the current study is the exposure route associated with sensitization and nanomaterial administration. The vast majority of existing studies have investigated the effects of metal nanomaterials when co-administered with antigen simultaneously during sensitization. Similar to the mechanisms of many commonly used vaccine adjuvants, the subsequent adjuvant effects are often dependent on particle/antigen interactions (Smith et al. 2013). Fewer studies have examined the potential adjuvant effects of metal nanomaterials when administered

independently from antigen (Han et al. 2011; Shen et al. 2011; 2012; Hsiao et al. 2018). Likewise, the current study was designed to determine if a particle exposure affected subsequent encounters with allergen, as may occur in occupational settings.

In this study, NiO particle effects appeared more prominent during the elicitation phase of the allergic response. Exposure-dependent variations in the OVA-specific IgE response only became apparent at 29 d, following two OVA challenges. IgE responses were consistent with the BAL fluid and serum cytokine profiles in the respective groups, which were also conserved with respect to NiO surface area (Figures 14 and 15; Table 5). The NiO-1A and NiO-2A groups trended together with a greater increase in Th2 cytokines while the NiO-3A group had greater increases in Th1 cytokine levels. This polarization pattern is also in accordance with the observation from histopathological analysis that multinucleated giant cells were exclusively present in the NiO-3A group. Giant cells have been associated with hard metal lung disease and Th1-dominant/delayed type hypersensitivity responses in the lung, including hypersensitivity pneumonitis (Bogaert et al. 2009; Wyman and Hines 2018).

The cellular profile of the mediastinal LN was another parameter shown to be correlated to the surface area of NiO in the OVA study (Figure 12). The 29 d LN response showed a similar trend between the NiO-1A and NiO-2A groups, where total cell number was increased over OVA controls, but the increase seen in the NiO-3A group was even further elevated over all other groups. Phenotypic analysis of LN cells revealed a pattern indicative of general expansion in the NiO-3A group, as all lymphocyte subpopulations were present in similar proportions as non-sensitized groups. Comparatively, a similar increase in the proportion of LN B-cells and decrease in the ratio of CD4+ T-cells was observed in the OVA, NiO-1A, and NiO-2A groups. These three groups exhibited alterations in LN cellular composition that would be expected in a typical IgE-mediated allergic condition, which was consistent with the increases in OVA-specific IgE levels seen in these animals. The lack of selective B-cell expansion in LN of the NiO-3A group also corresponded to the OVA-specific IgE response in the group, wherein levels were not elevated in a similar manner as the other sensitized groups. However, the NiO-3A group did exhibit significant increases in total IgE levels, which may have been reflective of the increase in absolute number of LN B-cells resulting from the drastic increase in LN size specifically observed in this group.

NiO nanoparticles, to our knowledge, have only been incorporated into one other asthma model to date. Horie et al. (2016) aspirated C57BL/6 mice with NiO nanoparticles (<100 nm) or microparticles (600 – 1400 nm), following which, mice were sensitized to OVA by inhalation (1, 3, 5, and 7 d post NiO exposure). Following four OVA challenges by inhalation (14, 16, 18, 20 d), OVA-specific IgE levels were increased exclusively in animals exposed to the smaller NiO particle (Horie et al. 2016).

The findings from our study and that of Horie et al. exhibit similarities, as well as discrepancies. In both studies, the treatment groups associated with increased production of OVA-specific IgE exhibited concurrent increases in Th2-dominant immune markers. In both studies, selective Th1/Th2 dominancy was also similarly related to NiO particle size and dose surface area. However, opposing effects of NiO size/surface area on the direction of Th1/Th2 polarization were reported by the two studies. This discrepancy may reflect the use of different mouse strains by the two studies, as the propensity for Th1/Th2-dominant immunity differs between BALB/c and C57BL/6 strains. Furthermore, clearance of nanoparticles from the lung is known to differ between these strains. Since the rate of NiO clearance appeared to contribute to variations in the LN response in the NiO time course study, this is a critical distinction between the studies that may account for the discordant findings (Jones et al. 2013).

Another source of variability between studies that may account for the divergent relationship between NiO size/surface area and Th1/Th2 polarization is the route of exposure used to induce OVA sensitization. Although both studies exposed animals to NiO via aspiration a day before sensitization, our study utilized intraperitoneal injections to induce sensitization, whereas Horie *et al.* induced sensitization by inhalation of OVA. As a result, the model design employed by Horie et al. uniquely facilitated the potential for interactions between NiO particles and OVA molecules in the lung during sensitization, whereas our study design was not conducive with the potential for similar interactions.

Many studies have shown that physical association of nanoparticles/antigen in the lungs during allergic sensitization can result in profound adjuvant effects (Brandenberger et al. 2013; Han et al. 2016). This response has been attributed to the binding of antigen/nanoparticles, which can result in altered antigen uptake and processing by APC, augmented delivery kinetics to the LN, regional deposition within the LN, and modulation of antigen presentation/lymphocyte stimulation. Accordingly, the magnitude of Th2 adjuvancy has been correlated to the surface loading capacity of nanoparticles, increases in which facilitate the binding of larger quantities of antigen. Physico-chemical properties of metal nanomaterials that have been associated with this mechanism of IgE/Th2 response amplification (when administered simultaneously with antigen during sensitization) include decreased particle size, increased surface area and porosity, and specific surface modifications (Yoshida et al. 2011; Han et al. 2016). The magnitude of Th2 adjuvant activity induced by many of these nanoparticles has also been shown to be dose-dependent, as larger doses facilitate the binding of higher quantities of antigen. Correspondingly, attenuation of metal nanomaterial-induced Th2 adjuvant activity has been correlated to increases in particle agglomeration, as well as surface properties associated with compromised antigen binding affinity/saturation (de Haar et al. 2006; Scarino et al. 2012; Ban et al. 2013). Collectively, these findings demonstrate that physical

interactions between antigen/nanoparticles can facilitate adjuvant effects on sensitization, and various physico-chemical properties of nanomaterials can further influence the magnitude of this effect. The association between decreased NiO particle size and increased OVA-specific IgE levels reported by Horie *et al.* is consistent with this mechanism of immunomodulation. Moreover, many of these studies have also demonstrated that the Th2 adjuvant activity of the nanomaterial is abolished if exposure occurs during the challenge phase of allergy. These findings highlight the existence of different mechanisms capable of augmenting allergic processes, and further emphasizes the importance of nanomaterial exposure occurrence with respect to the different phases of allergic disease (Meldrum et al. 2018; Vandebriel et al. 2018).

In contrast to the findings reported by Horie *et al.,* exposure to higher doses of NiO with respect to surface area caused exacerbation of Th1-driven inflammation in our OVA model. This effect was likely related to the persistent pro-inflammatory/Th1 pulmonary immune status in animals exposed to the high dose of NiO-UF on 0 d. As demonstrated in the NiO time course study, exposure to this dose (NiO-3 group) was associated with persistent elevations in several notable pro-inflammatory/Th1 cytokines (Figure 6) that were still significantly elevated at time points corresponding to time points of allergen challenge in the OVA model (19 and 29 d). The existence of an established Th1-polarized immune status in the airways could have limited the magnitude of allergen-induced Th2 responses mounted by the NiO-3A group, and/or further exacerbated the Th1 response. Comparatively, the resolution of NiO-induced pulmonary inflammation before OVA challenge in the NiO-1A and NiO-2A groups was associated with increases in OVA-specific IgE and Th2 cytokine levels. Several other studies have reported a similar induction of neutrophil-dominant lung inflammation by nanoparticles that correspondingly results in attenuation of Th2-driven allergic inflammation following systemic sensitization (Rossi et al. 2010; Jonasson et al. 2013; Shurin et al. 2014).

Differences in the routes of exposure employed by these two studies likely contributed to the conflicting findings regarding the impact of NiO size on the amplification of Th2-dominant allergic responses. This discriminating feature confers differential potential for particle/antigen interactions during sensitization, an effect which is known to impact the magnitude and nature of subsequent adaptive immune responses. Likewise, the findings from the two studies likely involve different immunological mechanisms of NiO-induced OVA allergy modulation, wherein these processes exhibit variations in susceptibility to influence from specific dose metrics and NiO particle characteristics. The correlation between decreased particle size and Th2 adjuvancy reported by Horie et al. is consistent with interactions between NiO/OVA in the lung during sensitization, leading to alterations in antigen delivery, and subsequent promotion of Th2-dominant response development. By comparison, the correlation between increased NiO surface area and Th1-dominant immune reactivity in our study is consistent with surface area-driven polarization of pulmonary immunity towards a pro-inflammatory state, predisposing for Th1-dominant reactivity upon allergen exposure.

In addition to the findings from these two asthma models, a few other studies have demonstrated results indicative of the potential for NiO nanoparticles to augment respiratory allergy by other mechanisms. For example, disruption in the pulmonary immune Th1/Th2 balance has been correlated to a varying degree of nitrative stress induced by different sizes of NiO nanoparticles (Chang et al. 2017). The preferential induction of Th1/Th17-dominant lung inflammation by NiO nanoparticles has been shown in numerous studies to cause the subsequent development of inflammatory reactions resembling delayed-type hypersensitivity reactions in the airways. Characteristic features of pulmonary alveolar proteinosis and hypersensitivity pneumonitis have been reported following NiO nanoparticle exposure *in vivo* (Cho et al. 2012a; Jeong et al. 2016a). Accordingly, respiratory exposure to NiO nanoparticles may present concerns with respect to both IgE-mediated and T-cell-mediated allergic responses in the lungs (Cho et al. 2010, 2012b; Cao et al. 2016).

The effect of NiO nanoparticles on allergic airway inflammation was examined in another study, where a T-bet$^{-/-}$ mouse model was used. This mouse model exhibits compromised Th1 cell development and subsequent predisposition for Th2-biased immunity, leading to the spontaneous generation of many pathophysiological characteristics of asthma, independent of allergen exposure. Many of these asthmatic features were shown to be exacerbated following exposure of mice to 20 nm NiO nanoparticles. Increased influx of lung eosinophils, mucus cell metaplasia, and elevations in Th2 cytokine levels were all observed, as well as chronic alveolitis. These findings suggest the potential for NiO nanoparticles to exacerbate Th2-driven inflammation in the elicitation phase of asthma, as well as potentially accelerate the development of airway remodeling in chronic asthmatic conditions (Glista-Baker et al. 2014).

Collectively, these existing studies emphasize that respiratory NiO nanoparticle exposure can modulate many aspects of pulmonary immunity. In naïve lungs, size-dependent skewing of immunity towards Th1 or Th2-dominancy may lead to the development of delayed-type hypersensitivity responses or enhance susceptibility for IgE-mediated allergic sensitization, respectively. Adjuvant effects on allergic sensitization and exacerbation of asthmatic elicitation responses can also emerge as a result of respiratory NiO exposure. Exacerbation of respiratory allergy can involve the modulation of any number of diverse immunological mechanisms, some of which are specific to the sensitization phase of allergy, whereas others are specific to the elicitation phase. Likewise, the immunomodulatory potential of NiO may differ depending on the sensitization status of the exposed individual. Moreover, as emphasized by the results from our study, specific physico-chemical properties may be differentially implicated in the immunological activity of NiO nanoparticles depending on the phase of allergic disease during which exposure occurs, the route of exposure, and the existence of concomitant disease states.

Conclusion

The results from the NiO time course study are consistent with existing studies, demonstrating a correlation between the surface area of metal nanomaterials and subsequent inflammatory response severity. However, the OVA study indicated that, in addition to surface area, other metrics related to NiO size were influential in the alteration of both local and systemic immune markers associated with IgE-dependent asthmatic responses. Further study is needed to determine role of dissolution as it relates to surface area and particle toxicity, particularly in different compartments in the lung such as acidic environments such is in the macrophage vacuoles. Since toxic effects of nanomaterials are heavily dependent on the biochemical properties of their environment, this observation emphasizes that the altered chemistry of asthmatic airways may implicate different mechanisms of toxicity than those typically observed in non-asthmatic lungs. This finding is likely applicable to other disease states, wherein the toxic effects of metal nanomaterials may be differentially correlated to physico-chemical properties in healthy and diseased tissues.

Disclaimer

The findings and conclusions in this article are those of the authors and do not necessarily represent the view of the National Institute for Occupational Safety and Health.

Disclosure statement

No potential conflict of interest was reported by the authors.

Funding

This work was supported by National Institute for Occupational Safety and Health and the American Foundation for Pharmaceutical Education.

References

ASTM International. 2002. Standard test method for metal powder specific surface area by physical adsorption. ASTM B922-10.

Bai KJ, Chuang KJ, Chen JK, Hua HE, Shen YL, Liao WN, Lee CH, Chen KY, Lee KY, Hsiao TC, et al. 2018. Investigation into the pulmonary inflammopathology of exposure to nickel oxide nanoparticles in mice. Nanomedicine. 14(7):2329–2339.

Ban M, Langonne I, Huguet N, Guichard Y, Goutet M. 2013. Iron oxide particles modulate the ovalbumin-induced Th2 immune response in mice. Toxicol Lett. 216(1):31–39.

Bezemer G. 2009. Particle deposition and clearance from the respiratory tract [master's thesis]. Utrecht University.

Bogaert P, Tournoy KG, Naessens T, Grooten J. 2009. Where asthma and hypersensitivity pneumonitis meet and differ: noneosinophilic severe asthma. Am J Pathol. 174(1):3–13.

Brandenberger C, Rowley NL, Jackson-Humbles DN, Zhang Q, Bramble LA, Lewandowski RP, Wagner JG, Chen W, Kaplan BL, Kaminski NE, et al. 2013. Engineered silica nanoparticles act as adjuvants to enhance allergic airway disease in mice. Part Fibre Toxicol. 10(1):26.

Brown DM, Dickson C, Duncan P, Al-Attili F, Stone V. 2010. Interaction between nanoparticles and cytokine proteins: impact on protein and particle functionality. Nanotechnology. 21(21):215104.

Cao Z, Fang Y, Lu Y, Qian F, Ma Q, He M, Pi H, Yu Z, Zhou Z. 2016. Exposure to nickel oxide nanoparticles induces pulmonary inflammation through NLRP3 inflammasome activation in rats. Int J Nanomedicine. 11:3331–3346.

Chang X, Zhu A, Liu F, Zou L, Su L, Li S, Sun Y. 2017. Role of NF-kappaB activation and Th1/Th2 imbalance in pulmonary toxicity induced by nano NiO. Environ Toxicol. 32(4):1354–1362.

Cho WS, Duffin R, Bradley M, Megson IL, MacNee W, Howie SEM, Donaldson K. 2012a. NiO and Co3O4 nanoparticles induce lung DTH-like responses and alveolar lipoproteinosis. Eur Respir J. 39(3):546–557.

Cho WS, Duffin R, Poland CA, Duschl A, Oostingh GJ, Macnee W, Bradley M, Megson IL, Donaldson K. 2012b. Differential pro-inflammatory effects of metal oxide nanoparticles and their soluble ions in vitro and in vivo; zinc and copper nanoparticles, but not their ions, recruit eosinophils to the lungs. Nanotoxicology. 6(1):22–35.

Cho WS, Duffin R, Poland CA, Howie SE, MacNee W, Bradley M, Megson IL, Donaldson K. 2010. Metal oxide nanoparticles induce unique inflammatory footprints in the lung: important implications for nanoparticle testing. Environ Health Perspect. 118(12):1699

Cockcroft DW, Davis B. 2006. Mechanisms of airway hyperresponsiveness. J Allergy Clin Immunol. 118(3):551–559.

de Haar C, Hassing I, Bol M, Bleumink R, Pieters R. 2006. Ultrafine but not fine particulate matter causes airway inflammation and allergic airway sensitization to co-administered antigen in mice. Clin Exp Allergy. 36(11):1469–1479.

De Jong WH, Van Der Ven LT, Sleijffers A, Park MV, Jansen EH, Van Loveren H, Vandebriel RJ. 2013. Systemic and immunotoxicity of silver nanoparticles in an intravenous 28 days repeated dose toxicity study in rats. Biomaterials. 34(33):8333–8343.

Glista-Baker EE, Taylor AJ, Sayers BC, Thompson EA, Bonner JC. 2014. Nickel nanoparticles cause exaggerated lung and airway remodeling in mice lacking the T-box transcription factor, TBX21 (T-bet). Part Fibre Toxicol. 11(1):7.

Gonzalez C, Salazar-Garcia S, Palestino G, Martinez-Cuevas PP, Ramirez-Lee MA, Jurado-Manzano BB, Rosas-Hernandez H, Gaytan-Pacheco N, Martel G, Espinosa-Tanguma R, et al. 2011. Effect of 45 nm silver nanoparticles (AgNPs) upon the smooth muscle of rat trachea: role of nitric oxide. Toxicol Lett. 207(3):306–313.

Han B, Guo J, Abrahaley T, Qin L, Wang L, Zheng Y, Li B, Liu D, Yao H, Yang J, et al. 2011. Adverse Effect of Nano-Silicon Dioxide on Lung Function of Rats with or without Ovalbumin Immunization. PLoS One. 6(2):e17236.

Han H, Park YH, Park HJ, Lee K, Um K, Park JW, Lee JH. 2016. Toxic and adjuvant effects of silica nanoparticles on ovalbumin-induced allergic airway inflammation in mice. Respir Res. 17(1):60.

Hirai T, Yoshikawa T, Nabeshi H, Yoshida T, Tochigi S, Ichihashi KI, Uji M, Akase T, Nagano K, Abe Y, et al. 2012. Amorphous silica nanoparticles size-dependently aggravate atopic dermatitis-like skin lesions following an intradermal injection. Part Fibre Toxicol. 9(1):3.

Ho M, Wu KY, Chein HM, Chen LC, Cheng TJ. 2011. Pulmonary toxicity of inhaled nanoscale and fine zinc oxide particles: mass and surface area as an exposure metric. Inhalation Toxicology. 23(14):947–956.

Horie M, Stowe M, Tabei M, Kuroda E. 2016. Metal ion release of manufactured metal oxide nanoparticles is involved in the allergic response to inhaled ovalbumin in mice. ODEM. 04(02):17.

Horie M, Fukui H, Endoh S, Maru J, Miyauchi A, Shichiri M, Fujita K, Niki E, Hagihara Y, Yoshida Y, et al. 2012. Comparison of acute oxidative stress on rat lung induced by nano and fine-scale, soluble and insoluble metal oxide particles: NiO and TiO2. Inhalation Toxicology. 24(7):391–400.

Horie M, Fukui H, Nishio K, Endoh S, Kato H, Fujita K, Miyauchi A, Nakamura A, Shichiri M, Ishida N, et al. 2011. Evaluation of acute

oxidative stress induced by NiO nanoparticles in vivo and in vitro. J Occup Health. 53(2):64–74.
Hsiao YP, Shen CC, Huang CH, Lin YC, Jan TR. 2018. Iron oxide nanoparticles attenuate T helper 17 cell responses in vitro and in vivo. Int Immunopharmacol. 58:32–39.
Hunt JF, Fang K, Malik R, Snyder A, Malhotra N, Platts-Mills TA, Gaston B. 2000. Endogenous airway acidification: implications for asthma pathophysiology. Am J Respir Crit Care Med. 161(3): 694–699.
Hussain S, Boland S, Baeza-Squiban A, Hamel R, Thomassen LC, Martens JA, Billon-Galland MA, Fleury-Feith J, Moisan F, Pairon JC, et al. 2009. Oxidative stress and proinflammatory effects of carbon black and titanium dioxide nanoparticles: role of particle surface area and internalized amount. Toxicology. 260(1–3):142–149.
ICRP. 1994. Human respiratory tract model for radiological protection. ICRP Publication 66. Ann ICRP. 24(1–3).
Ilves M, PalomäKi J, Vippola M, Lehto M, Savolainen K, Savinko T, Alenius H. 2014. Topically applied ZnO nanoparticles suppress allergen induced skin inflammation but induce vigorous IgE production in the atopic dermatitis mouse model. Part Fibre Toxicol. 11(1):38.
Ingham E, Fisher J. 2000. Biological reactions to wear debris in total joint replacement. Proc Inst Mech Eng H. 214(1):21–37.
Jeong J, Han Y, Poland CA, Cho WS. 2015. Response-metrics for acute lung inflammation pattern by cobalt-based nanoparticles. Part Fibre Toxicol. 12(1):13.
Jeong J, Kim J, Seok SH, Cho WS. 2016a. Indium oxide (In 2 O 3) nanoparticles induce progressive lung injury distinct from lung injuries by copper oxide (CuO) and nickel oxide (NiO) nanoparticles. Arch Toxicol. 90(4):817–828.
Jeong J, Lee S, Kim SH, Han Y, Lee DK, Yang JY, Jeong J, Roh C, Huh YS, Cho WS. 2016b. Evaluation of the dose metric for acute lung inflammogenicity of fast-dissolving metal oxide nanoparticles. Nanotoxicology. 10(10):1448–1457.
Jonasson S, Gustafsson A, Koch B, Bucht A. 2013. Inhalation exposure of nano-scaled titanium dioxide (TiO2) particles alters the inflammatory responses in asthmatic mice. Inhal Toxicol. 25(4):179–191.
Jones SW, Roberts RA, Robbins GR, Perry JL, Kai MP, Chen K, Bo T, Napier ME, Ting JPY, DeSimone JM, et al. 2013. Nanoparticle clearance is governed by Th1/Th2 immunity and strain background. J Clin Invest. 123(7):3061–3073.
Kapilevich LV, Zaĭtseva TN, Nosarev AV, D'iakova EI, Petlina ZR, Ogorodova LM, Ageev BG, Magaeva AA, Itin VI, Terekhova OG, et al. 2012. Influence of nanosize particles of cobalt ferrite on contractile responses of smooth muscle segment of airways. Ross Fiziol Zh Im I M Sechenova. 98(2):228–235.
Kato M, Suzuki M, Hayashi Y, Kimura H. 2006. Role of eosinophils and their clinical significance in allergic inflammation. Expert Rev Clin Immunol. 2(1):121–133.
Klink K, Meade B. 2003. Dermal exposure to 3-amino-5-mercapto-1, 2, 4-triazole (AMT) induces sensitization and airway hyperreactivity in BALB/c mice. Toxicol Sci. 75(1):89–98.
Kuempel E, Castranova V, Geraci C, Schulte P. 2012. Development of risk-based nanomaterial groups for occupational exposure control. J Nanopart Res. 14(9):1029.
Lee S, Hwang SH, Jeong J, Han Y, Kim SH, Lee DK, Lee HS, Chung ST, Jeong J, Roh C, et al. 2016. Nickel oxide nanoparticles can recruit eosinophils in the lungs of rats by the direct release of intracellular eotaxin. Part Fibre Toxicol. 13(1):30.
Lee S, Yun HS, Kim SH. 2011. The comparative effects of mesoporous silica nanoparticles and colloidal silica on inflammation and apoptosis. Biomaterials. 32(35):9434–9443.
Lehmann S, Gilbert B, Maffeis T, Grichine A, Pignot-Paintrand I, Clavaguera S, Rachidi W, Seve M, Charlet L. 2018. In Vitro Dermal Safety Assessment of Silver Nanowires after Acute Exposure: Tissue vs. Cell Models. 8(4):232.
Li X, Aldayel AM, Cui Z. 2014. Aluminum hydroxide nanoparticles show a stronger vaccine adjuvant activity than traditional aluminum hydroxide microparticles. J Control Release. 173:148–157.
Lin F, Zhang H, Huang J, Xiong C. 2018. Contractility of Airway Smooth Muscle Cell in Response to Zinc Oxide Nanoparticles by Traction Force Microscopy. Ann Biomed Eng. 46(12):2000–2011.
Marques MR, Loebenberg R, Almukainzi M. 2011. Simulated biological fluids with possible application in dissolution testing. Dissolution Technol. 18(3):15–28.
McBrien CN, Menzies-Gow A. 2017. The Biology of Eosinophils and Their Role in Asthma. Front Med. 4:93–93.
Meldrum K, Guo C, Marczylo EL, Gant TW, Smith R, Leonard MO. 2017. Mechanistic insight into the impact of nanomaterials on asthma and allergic airway disease. Part Fibre Toxicol. 14(1):45.
Meldrum K, Robertson SB, Römer I, Marczylo T, Dean LSN, Rogers A, Gant TW, Smith R, Tetley TD, Leonard MO. 2018. Cerium dioxide nanoparticles exacerbate house dust mite induced type II airway inflammation. Part Fibre Toxicol. 15(1):24.
Misharin AV, Morales-Nebreda L, Mutlu GM, Budinger GRS, Perlman H. 2013. Flow Cytometric Analysis of Macrophages and Dendritic Cell Subsets in the Mouse Lung. Am J Respir Cell Mol Biol. 49(4): 503–510.
Mizuguchi Y, Myojo T, Oyabu T, Hashiba M, Lee BW, Yamamoto M, Todoroki M, Nishi K, Kadoya C, Ogami A, et al. 2013. Comparison of dose-response relations between 4-week inhalation and intratracheal instillation of NiO nanoparticles using polimorphonuclear neutrophils in bronchoalveolar lavage fluid as a biomarker of pulmonary inflammation. Inhal Toxicol. 25(1):29–36.
Mo Y, Jiang M, Zhang Y, Wan R, Li J, Zhong CJ, Li H, Tang S, Zhang Q. 2019. Comparative mouse lung injury by nickel nanoparticles with differential surface modification. J Nanobiotechnology. 17(1):2.
Morimoto Y, Hirohashi M, Ogami A, Oyabu T, Myojo T, Hashiba M, Mizuguchi Y, Kambara T, Lee BW, Kuroda E, Tanaka I. 2011. Pulmonary toxicity following an intratracheal instillation of nickel oxide nanoparticle agglomerates. J Occup Health. 53(4):293–295.
Morimoto Y, Ogami A, Todoroki M, Yamamoto M, Murakami M, Hirohashi M, Oyabu T, Myojo T, Nishi KI, Kadoya C, et al. 2010. Expression of inflammation-related cytokines following intratracheal instillation of nickel oxide nanoparticles. Nanotoxicology. 4(2): 161–176.
Oberdorster G, Ferin J, Morrow PE. 1992. Volumetric loading of alveolar macrophages (AM): a possible basis for diminished AM-mediated particle clearance. Exp Lung Res. 18(1):87–104.
Ogami A, Morimoto Y, Murakami M, Myojo T, Oyabu T, Tanaka I. 2009a. Biological effects of nano-nickel in rat lungs after administration by inhalation and by intratracheal instillation. J Phys Conf Ser. 151(1):012032.
Ogami A, Morimoto Y, Myojo T, Oyabu T, Murakami M, Todoroki M, Nishi K, Kadoya C, Yamamoto M, Tanaka I. 2009b. Pathological features of different sizes of nickel oxide following intratracheal instillation in rats. Inhal Toxicol. 21(10):812–818.
Ortega VA, Ede JD, Boyle D, Stafford JL, Goss GG. 2015. Polymer-coated metal-oxide nanoparticles inhibit IgE receptor binding, cellular signaling, and degranulation in a mast cell-like cell line. Adv Sci. 2(11):1500104.
Park EJ, Bae E, Yi J, Kim Y, Choi K, Lee SH, Yoon J, Lee BC, Park K. 2010. Repeated-dose toxicity and inflammatory responses in mice by oral administration of silver nanoparticles. Environ Toxicol Pharmacol. 30(2):162–168.
Poland CA, Byrne F, Cho WS, Prina-Mello A, Murphy FA, Davies GL, Coey JM, Gounko Y, Duffin R, Volkov Y, et al. 2012. Length-dependent pathogenic effects of nickel nanowires in the lungs and the peritoneal cavity. Nanotoxicology. 6(8):899–911.
Porter D, Sriram K, Wolfarth M, Jefferson S, Schwegler-Berry D, Andrew ME, Castranova V. 2008. A biocompatible medium for nanoparticle dispersion. Nanotoxicology. (3):144. 2
Radauer-Preiml I, Andosch A, Hawranek T, Luetz-Meindl U, Wiederstein M, Horejs-Hoeck J, Himly M, Boyles M, Duschl A. 2016. Nanoparticle-allergen interactions mediate human allergic responses: protein corona characterization and cellular responses. Part Fibre Toxicol. 13(1):3.

Rankin SM, Conroy DM, Williams T. 2000. Eotaxin and eosinophil recruitment: implications for human disease. Mol Med Today. 6(1): 20–27.

Roach KA, Stefaniak AB, Roberts JR. 2019. Metal nanomaterials: immune effects and implications of physicochemical properties on sensitization, elicitation, and exacerbation of allergic disease. J Immunotoxicol. 16(1):87–124.

Rossi EM, Pylkkanen L, Koivisto AJ, Nykasenoja H, Wolff H, Savolainen K, Alenius H. 2010. Inhalation exposure to nanosized and fine TiO2 particles inhibits features of allergic asthma in a murine model. Part Fibre Toxicol. 7(1):35.

Roy R, Kumar S, Verma AK, Sharma A, Chaudhari BP, Tripathi A, Das M, Dwivedi PD. 2014. Zinc oxide nanoparticles provide an adjuvant effect to ovalbumin via a Th2 response in Balb/c mice. Int Immunol. 26(3):159–172.

Sager TM, Castranova V. 2009. Surface area of particle administered versus mass in determining the pulmonary toxicity of ultrafine and fine carbon black: comparison to ultrafine titanium dioxide. Part Fibre Toxicol. 6(1):15.

Sager T, Kommineni C, Castranova V. 2008. Pulmonary response to intratracheal instillation of ultrafine versus fine titanium dioxide: Role of surface area. Part Fibre Toxicol. 5(1):17.

Sager T, Wolfarth M, Keane M, Porter D, Castranova V, Holian A. 2016a. Effects of nickel-oxide nanoparticle pre-exposure dispersion status on bioactivity in the mouse lung. Nanotoxicology. 10(2): 151–161.

Sager TM, Wolfarth M, Leonard SS, Morris AM, Porter DW, Castranova V, Holian A. 2016b. Role of engineered metal oxide nanoparticle agglomeration in reactive oxygen species generation and cathepsin B release in NLRP3 inflammasome activation and pulmonary toxicity. Inhal Toxicol. 28(14):686–697.

Scarino A, Noel A, Renzi P, Cloutier Y, Vincent R, Truchon G, Tardif R, Charbonneau M. 2012. Impact of emerging pollutants on pulmonary inflammation in asthmatic rats: ethanol vapors and agglomerated TiO2 nanoparticles. Inhal Toxicol. 24(8):528–538.

Schinwald A, Chernova T, Donaldson KJP, Toxicology F. 2012. Use of silver nanowires to determine thresholds for fibre length-dependent pulmonary inflammation and inhibition of macrophage migration in vitro. Part Fibre Toxicol. 9(1):47.

Schinwald A, Donaldson K. 2012. Use of back-scatter electron signals to visualise cell/nanowires interactions in vitro and in vivo; frustrated phagocytosis of long fibres in macrophages and compartmentalisation in mesothelial cells in vivo. Part Fibre Toxicol. 9(1):34–34.

Schmid O, Stoeger T. 2016. Surface area is the biologically most effective dose metric for acute nanoparticle toxicity in the lung. J Aerosol Sci. 99:133–143.

Schneider L, Hanifin J, Boguniewicz M, Eichenfield LF, Spergel JM, Dakovic R, Paller AS. 2016. Study of the atopic march: development of atopic comorbidities. Pediatr Dermatol. 33(4):388–398.

Shen CC, Liang HJ, Wang CC, Liao MH, Jan TR. 2012. Iron oxide nanoparticles suppressed T helper 1 cell-mediated immunity in a murine model of delayed-type hypersensitivity. Int J Nanomedicine. 7:2729–2737.

Shen CC, Wang CC, Liao MH, Jan TR. 2011. A single exposure to iron oxide nanoparticles attenuates antigen-specific antibody production and T-cell reactivity in ovalbumin-sensitized BALB/c mice. Int J Nanomedicine. 6:1229.

Shurin MR, Yanamala N, Kisin ER, Tkach AV, Shurin GV, Murray AR, Leonard HD, Reynolds JS, Gutkin DW, Star A, et al. 2014. Graphene oxide attenuates Th2-type immune responses, but augments airway remodeling and hyperresponsiveness in a murine model of asthma. ACS Nano. 8(6):5585–5599.

Smith DM, Simon JK, Baker JR Jr. 2013. Applications of nanotechnology for immunology. Nat Rev Immunol. 13(8):592–605.

Stoeger T, Reinhard C, Takenaka S, Schroeppel A, Karg E, Ritter B, Heyder J, Schulz H. 2006. Instillation of six different ultrafine carbon particles indicates a surface area threshold dose for acute lung inflammation in mice. Environ Health Perspect. 114(3):328–333.

Toda T, Yoshino S. 2016. Enhancement of ovalbumin-specific Th1, Th2, and Th17 immune responses by amorphous silica nanoparticles. Int J Immunopathol Pharmacol. 29(3):408–420.

Vance ME, Kuiken T, Vejerano EP, McGinnis SP, Hochella MF, Rejeski D, Hull MS. 2015. Nanotechnology in the real world: redeveloping the nanomaterial consumer products inventory. Beilstein J Nanotechnol. 6:1769–1780.

Vandebriel RJ, Vermeulen JP, van Engelen LB, de Jong B, Verhagen LM, de la Fonteyne-Blankestijn LJ, Hoonakker ME, de Jong WH. 2018. The crystal structure of titanium dioxide nanoparticles influences immune activity in vitro and in vivo. Part Fibre Toxicol. 15(1):9.

VanOs R, Lildhar LL, Lehoux EA, Beaule PE, Catelas I. 2014. In vitro macrophage response to nanometer-size chromium oxide particles. J Biomed Mater Res Part B Appl Biomater. 102(1):149–159.

Woolhiser MR, Munson AE, Meade BJ. 2000. Comparison of mouse strains using the local lymph node assay. Toxicology. 146(2–3): 221–227.

Wyman AE, Hines SE. 2018. Update on metal-induced occupational lung disease. Curr Opin Allergy Clin Immunol. 18(2):73–79.

Yoshida T, Yoshioka Y, Fujimura M, Yamashita K, Higashisaka K, Morishita Y, Kayamuro H, Nabeshi H, Nagano K, Abe Y, et al. 2011. Promotion of allergic immune responses by intranasally-administrated nanosilica particles in mice. Nanoscale Res Lett. 6(1): 195.

Zhang Q, Kusaka Y, Zhu X, Sato K, Mo Y, Kluz T, Donaldson K. 2003. Comparative toxicity of standard nickel and ultrafine nickel in lung after intratracheal instillation. Jrnl of Occup Health. 45(1): 23–30.